This is a preprint, the final version is subject to change, of the American Mineralogist (MSA)
Cite as Authors (Year) Title. American Mineralogist, in press.
DOI: https://doi.org/10.2138/am-2018-6415

Submission to the *American Mineralogist (Special Issue dedicated to Biomaterials) - Manuscript Revision 1*

Nanocrystalline apatites: the fundamental role of water

Christophe Drouet[a,*], Maëlenn Aufray[a], Sabrina Rollin-Martinet[a,b], Nicolas Vandecandelaère[a], David Grossin[a], Fabrice Rossignol[b], Eric Champion[b], Alexandra Navrotsky[c], Christian Rey[a]

[a]CIRIMAT, Université de Toulouse, UMR CNRS/INPT/UPS 5085, ENSIACET, 4 allee Emile Monso, 31030 Toulouse cedex 4, France (Corresponding author, E-mail: christophe.drouet@cirimat.fr; Phone: +33 (0)6 19 99 77 36)

[b]Université de Limoges, CNRS, SPCTS, UMR 7315, Centre Européen de la Céramique, 12 rue Atlantis, 87068 Limoges cedex, France (E-mail: eric.champion@unilim.fr)

[c]Peter A. Rock Thermochemistry Laboratory and NEAT ORU, University of California Davis, 1 Shields Ave., Davis CA 95616 USA (E-mail: anavrotsky@ucdavis.edu; Phone: 530 752 3292; Fax: 530 752 9307)

Main corresponding Author:

Christophe Drouet
CIRIMAT Institute – UMR CNRS 5085
ENSIACET
4 allee Emile Monso
31030 Toulouse cedex 4, France

E-mail: christophe.drouet@cirimat.fr
Phone: +33 (0)6 19 99 77 36

Abstract

Bone is a natural nanocomposite. Its mineral component is nanocrystalline calcium phosphate apatite, whose synthetic biomimetic analogs can be prepared by wet chemistry. The initially formed crystals, whether biological or synthetic, exhibit very peculiar physicochemical features. In particular, they are nanocrystalline, nonstoichiometric and hydrated. The surface of the nanocrystals is covered by a non-apatitic hydrated layer with mobile ions, which may explain their exceptional surface reactivity. For their precipitation *in vivo* or *in vitro*, for their evolution in solution, for the evolving 3D organization of the nanocrystals, and for their consolidation to obtain bulk ceramic materials, water appears to be a central component that has not received much attention. In this mini-review, we explore these key roles of water on the basis of physicochemical and thermodynamic data obtained by complementary tools including FTIR, XRD, ion titrations, oxide melt solution calorimetry, and cryo-FEG-SEM. We also report new data obtained by DSC, aiming to explore the types of water molecules associated with the nanocrystals. These data support the existence of two main types of water molecules associated with the nanocrystals, with different characteristics and probably different roles and functions. These findings improve our understanding of the behavior of bioinspired apatite-based systems for biomedicine and also of biomineralization processes taking place *in vivo*, at present and in the geologic past. This paper is thus intended to give an overview of the specificities of apatite nanocrystals and their close relationship with water.

Keywords: Nanocrystalline apatite, Water, Hydroxyapatite, Bone, DSC, cryo SEM, Thermodynamics, Enthalpy

Introduction

Nanocrystalline apatites constitute the mineral portion of bone and dentin (Gomez-Morales et al., 2013; LeGeros and LeGeros, 1984). In these biominerals, nanocrystals are composed of a crystalline core of nonstoichiometric calcium phosphate apatite, deriving from hydroxyapatite $Ca_{10}(PO_4)_6(OH)_2$ and containing trace amounts of other mineral ions such as sodium, strontium, fluoride etc. This core is covered by a non-apatitic ionic hydrated layer (Cazalbou et al., 2004a; Eichert et al., 2005,2008; Jäger et al., 2006; Rey et al., 1989,1990,2007; Grossin et al, 2010; Vandecandelaere et al., 2012; Gomez-Morales et al., 2013; Wang et al., 2013), conferring exceptional surface reactivity which is exploited *in vivo* for regulating ionic concentrations in body fluids in homeostasis processes (Bonjour, 2011; Rey et al., 1989, 1990, 2009; Driessens et al., 1986). The overall composition of bone apatite can generally be rather satisfactorily described as $Ca_{10-x}(PO_4)_{6-x}(HPO_4,CO_3)_x(OH,½CO_3)_{2-x}$ with $0 \leq x \leq 2$ (Eichert et al., 2008; Rey et al., 2009), and compilation of cortical bone analyses suggested the following averaged chemical composition (Legros et al., 1987): $Ca_{8.3}(PO_4)_{4.3}(HPO_4,CO_3)_{1.7}(OH,½CO_3)_{0.3}$. In these formulas, carbonation can be present by substitution of hydroxyl groups in the so-called apatitic-channels of the lattice (A-type carbonates) or of phosphate groups (B-type). Labile carbonate (LC) species corresponding to surface carbonate ions within the surface layer can also be identified. The overall degree of carbonation is low for early, immature apatitic deposits, but it progressively increases up to several weight percents upon aging. For charge compensation, some PO_4^{3-} ions are substituted by HPO_4^{2-} ions (which, in the apatitic lattice, occupy the same type of sites as B-type carbonates).

It is possible to prepare biomimetic analogs to bone apatite, either carbonate-substituted or non-carbonated, by soft chemistry using close-to-physiological synthesis routes such as coprecipitation (Delgado-Lopez et al., 2012; Iafisco et al., 2011, 2012; Vandecandelaere et al.,

2012; Pasteris et al., 2012). These synthetic compounds not only help us to understand biomineralization phenomena, but also encourage the development of bio-inspired materials for bone regeneration and, more recently, in nanomedicine, e.g., for oncology (Drouet et al., 2015; Kramer et al., 2014; Iafisco et al., 2012, 2013; Bouladjine et al., 2009), gene delivery (Hossain et al., 2010; Sokolova et al., 2006; Chowdhury and Akaike, 2005) and hematology (Stefanic et al., 2017). For such applications, raw precipitates must be processed into either 3D scaffolds, 2D surface coatings on appropriate substrates, or even 1D individualized nanoparticles; this processing step may lead to non-negligible modifications of the initial nanocrystals.

Whether for synthesis by precipitation in aqueous solution, nanocrystal evolution in solution or in natural bone environment *in vivo*, or biomaterials processing (potentially involving drying, consolidation and sterilization steps), one actor remains ubiquitous: water. This component indeed appears as a major ingredient for deciphering apatite nanocrystal formation and fate in humid conditions. However, to date, focus has rarely been placed on this "constituent of life" from a physicochemical point of view when dealing with apatite.

In such nonstoichiometric apatite compounds, water molecules could possibly occupy several sites: on the surface of the crystals (within the hydrated ionic layer), but also possibly in some ion vacancies in the lattice (vacancies in OH sites, in calcium sites, or in the oxygen vacancy left in phosphate sites by the CO_3-for-PO_4 substitution in the case of B-type carbonate). **Figure 1** shows in a schematic way the possible positions of ion vacancies in the apatite lattice. Neuman et al. (1953a,b) discussed the hydration state of bone and synthetic apatite, and mentioned that "the water associated with the crystals of both synthetic hydroxyl apatite and bone when in aqueous media does not appear to be due either to capillary condensation or to the formation of a crystalline hydrate", thus suggesting a different involvement of water molecules, although they concluded that "the concept of the hydration

shell requires considerable clarification". In his review, Glimcher (1959) pointed out for precipitated apatites the presence of "excess water [that] cannot be separated from the crystals by mechanical centrifugation at 80 000 g", later referring to water being part of "a large hydration shell of water 'bound' to the crystals", and concluded by adding: "the very large surface tension and capillarity effects between such crystal surfaces could well 'trap' a large amount of water in addition to a bound monolayer, and still resist separation from the crystals by mechanical centrifugation". These conclusions underlined the ubiquitous presence of water, although no clarification of the type of interactions with the mineral was presented. By way of birefringence measurements at various temperatures from 60 ° to 400°C for 2-hour periods, Carlström et al. (1963) examined the water bound to enamel and concluded the existence of two different types: one "very loosely bound" that they attributed to the organic matrix and a larger part "firmly bound to the mineral phase". However no details were given on the water specifically linked to the mineral. Also that report dealt with relatively large enamel crystals, closer to stoichiometric hydroxyapatite than bone crystals. In bone, Timmins and Wall (1977) reported a review on the presence of water associated more or less strongly with the tissue, but no experimental data were given for the water related to the mineral phase. LeGeros et al. (1978) reported some data for water associated to enamel and precipitated apatites, for which they pointed out two types of associated water, referred to as "adsorbed" and "lattice" water, released sequentially upon heating. The latter authors considered the "adsorbed" water as of the water type previously considered by Carlström as linked to the organic matrix, and they attributed the "lattice" water to "H_2O-for-OH" and/or "HPO_4-for-PO_4" substitutions in the apatitic lattice. Taking into account their heating conditions (to 400 °C at 5 °C/min), the decomposition of HPO_4^{2-} ions from the lattice is indeed expected to generate H_2O molecules either in condensation to form pyrophosphate ($P_2O_7^{4-}$) ions or in reaction with carbonate ions to give CO_2 and H_2O. However, again, little is known about the

water initially present (not formed upon decomposition of other chemical species). Starting in 2006, cold sintering (e.g. spark plasma sintering) was applied to nanocrystalline apatites (Drouet et al., 2006, 2009; Grossin et al., 2010), pointing out the possibility to consolidate these compounds at low temperature, typically around 150 °C. To explain this possibility despite a low thermal activation of ion diffusion in these conditions, the role of the hydrated layer, and thus of water, was then evidenced for the first time. Indeed, a high mobility of the ions contained in surface hydrated environments is thought to allow ion diffusion and therefore to favor crystal-crystal interactions despite the low temperature. Rollin-Martinet et al. (2011) realized cryo-FEG-SEM analyses of synthetic apatite nanocrystals during the precipitation stage, unveiling the formation of bundles of aligned nanocrystals surrounded by a seemingly amorphous shell suspected to be water-rich. Wang et al. (2013) reported a similar role of water in the orientation of apatite crystals in bone tissue. They also concluded that "structuring water molecules strongly interact with the mineral when a disordered mineral layer coats the crystalline core of the mineral particles". This statement parallels the conclusions drawn from low temperature sintering experiments; indeed, in both cases (in bone and for the consolidation of nanocrystalline apatites), the organization of the nanocrystals is linked to (controlled by?) the hydrated layer present on the nanocrystals. Also, the "disordered mineral layer" corresponds perfectly to the hydrated and ionic surface layer present on the nanocrystals previously reported (Vandecandelaere et al., 2012; Kaflak and Kolodziejski, 2008; Cazalbou et al., 2004a, 2004b; Lu et al., 2000; Rey et al., 1989, 1990; Roufosse et al., 1984). Granke et al. (2015) explored the mechanical behavior of bone and related it to its water content to complement other works on this topic (Unal and Akkus, 2015; Nyman et al., 2006). In addition, Nyman et al. (2008) developed an NMR-based methodology to follow the "mobile" and "bound" water associated with human femurs; where "mobile" water is considered to fill microscopic pores (found in Haversian canals, canaliculi, and lacunae) while

"bound water" refers to a "structural water layer bridging mineral and collagen". The eventuality of different types of water molecules was also reported by Wilson et al. (2005, 2006) from NMR experiments, where water was suspected to "occupy the vacancies created by substitutions and defects in the crystal lattice" but also to be involved in more superficial chemical environments for mediating mineral-organic matrix interactions. Yoder et al. (2012a,b) and Pasteris et al. (2014), reported NMR, TGA and Raman spectroscopy data on carbonated apatites and interpreted them by considering that water molecules resided in apatite channels, although no direct correlation was found in these works between the density of vacancies and the amount of water incorporated in the apatite lattice. In older works, using essentially TGA, LeGeros et al. (1979) and Labarthe et al. (1973) reported also on water trapped in the lattice of type B carbonated apatites, considered to be associated with oxygen vacancies in sodium-free carbonated apatites but independent of the carbonate content in sodium-containing carbonated apatites as confirmed by Pasteris et al. (2014). The presence of incorporated water in nonstoichiometric apatites has also been proposed on the basis of Rietveld refinement of XRD data as in Ivanova et al. (2001), either in apatite channels or in replacement of the oxygen vacancy left by substituting PO_4 by CO_3.

As can be seen from the above, water appears strongly involved in mineralized tissues, including substantial interaction with the mineral component, although several conceptions have been expressed along the years (water associated to the organic component, water in porosity, water from the hydrated layer, adsorbed water, water in OH vacancies or in calcium vacancies or in the oxygen vacancies in the lattice,…), as summarized chronologically by Pasteris (2012). Today, the water-mineral system requires specific attention more than ever, with consideration of several complementary aspects involving water and apatite nanocrystals. In the present mini-review, we wish to give water the central role it deserves, by providing a global picture of the fundamental role that it plays in the genesis, evolution, and

interaction schemes involving apatite nanocrystals. For easier reading, the text is divided into several successive subsections referring to the synthesis of the nanocrystals and their evolution in solution (including thermodynamic aspects), the impact of drying, the exploration of the different "types" of water molecules associated with the nanocrystals, the role of water in the 3D organization of the nanocrystals, their consolidation at "low" temperature by cold sintering to obtain bioceramics, and finally some considerations relevant to the *in vivo* setting.

Materials and Methods

Biomimetic apatites were produced and characterized by TEM, FTIR, XRD and TGA as described previously (Vandecandelaere et al., 2012).

Differential scanning calorimetry (DSC) was performed using a DSC 204 Phoenix Series (Netzsch, Selb, Germany) coupled with a TASC 414/4 controller. The apparatus was calibrated against melting temperatures of In, Hg, Sn, Bi, CsCl, and Zn, applying two 10 °C/min temperature ramps, as recommended (Della Gatta et al., 2006). The calibration was verified before each experiment using indium, with an accuracy of ± 0.5 °C and ± 0.5 J/g. The samples were placed in stainless steel capsules (120 μL) and the mass was measured with an accuracy of ± 0.1 mg. The samples were heated from –50 to 300 °C at 10 °C/min under a continuous flow of nitrogen.

A field-emission-gun scanning electron microscope (JEOL 7400) equipped with a cryogenic system (Gatan Alto 2500), or "Cryo-FEG-SEM", was used to examine the morphology of freshly precipitated, wet apatite nanocrystals at various timepoints during their maturation in solution. For each analysis, one droplet was sampled with a pipette out of the precipitating medium and deposited on the sample holder. The system was then frozen and transferred into a chamber cooled with liquid nitrogen.

Technical details on the consolidation of nanocrystalline apatites by cold sintering and related mechanical testing were reported by Grossin et al. (2010). The relative density of the samples was calculated from the ratio between their apparent density (evaluated from the dimensions of the consolidated cylindrical pellets and their mass) and their true density (determined by He pycnometry with a Micromeritics AccuPyc 1330 apparatus, with 10 successive measurements on each sample).

Ion exchange was carried out by immersing 200 mg of nanocrystalline apatite sample in 50 ml of a 1 M aqueous solution of magnesium chloride $MgCl_2.6H_2O$, at room temperature under stirring, for 30 min. The suspension was then filtered, washed with deionized water and freeze-dried. Ca and Mg concentrations were then determined by ICP-AES analyses (uncertainty on alkaline-earth titration: 5%).

High temperature oxide melt calorimetry was carried out in a Tian-Calvet twin calorimeter, as previously described (Rollin-Martinet et al., 2013; Ushakov et al., 2001). A minimum of 8 values were obtained for each composition, and uncertainties are two standard deviations of the mean.

Results and Discussion

Synthesis of nanocrystalline apatites via wet chemistry

Apatite samples precipitated at moderate temperature, typically under the boiling point of the solution, generally exhibit a nonstoichiometric chemical composition, with less calcium and hydroxide than the theoretical hydroxyapatite (HAP) formula $Ca_{10}(PO_4)_6(OH)_2$ (Gomez-Morales et al., 2013; LeGeros and LeGeros, 1984). Although the preparation of stoichiometric HAP in the dry state can be done rather easily by calcining in (moist) air a variety of reactants used in stoichiometric proportions, e.g., by mixing $CaCO_3$ and beta tricalcium phosphate

$Ca_3(PO_4)_2$ (Elliott, 1994), obtaining truly stoichiometric HAP from wet chemistry is a delicate process as calcium and hydroxide crystallographic sites need to be completely filled. This is generally realized at (or close to) boiling temperature, under alkaline pH, and usually via dropwise addition of the calcium and phosphate reactants under constant stirring (Raynaud et al., 2002). Therefore, many wet syntheses of apatite – especially in mild conditions close to physiological – produce nonstoichiometric compositions. This is the case in bone *in vivo*, and also in the preparation of biomimetic analogs (Vandecandelaere et al., 2012). For instance, chemical titrations for an apatite matured 1 day at 22 °C and pH 7.2 (prior to filtration and freeze-drying) resulted in the mean composition $Ca_{8.64}(PO_4)_{4.88}(HPO_4)_{1.12}(OH)_{0.39}$, corresponding to a Ca/P molar ratio of 1.44 ± 0.02, significantly lower than the value of 1.67 for stoichiometric HAP. An example of samples precipitated at 22°C is given in **Figure 2**. TEM observation (**Figure 2a**) confirms the nanometric dimensions of the constitutive crystals, and shows an elongated crystal shape with a tendency to form platelets. X-ray diffraction (XRD) analysis reveals (**Figure 2b**) the low intensity and large FWHM of the peaks when compared to well-crystallized stoichiometric HAP (Vandecandelaere et al., 2012; Grynpas, 1976). This low crystallinity can be attributed both to the nanometric size of the crystals and to the existence of internal crystal strain due to nonstoichiometry and other point defects in the crystal. Additionally, Fourier transform infrared (FTIR) spectroscopy of biomimetic nanocrystalline apatite detects (**Figure 2c**) not only the characteristic vibrations of calcium phosphate apatite, but also an enhanced contribution of water molecules, as evidenced by a broad band in the range 2700-3500 cm^{-1} assignable to O-H stretching in H_2O, as well as an increase of the HOH bending contribution of water at 1640 cm^{-1}. Moreover, as for bone apatite (Rey et al., 1990), other spectral features differ from those of well-crystallized stoichiometric HAP. This is particularly visible in the $\nu_4(PO_4)$ spectral domain where, in addition to the libration band of apatitic OH^- ions around 632 cm^{-1} and the three

typical contributions of apatitic PO_4^{3-} groups (around 601, 575 and 560 cm^{-1}, marked in red on **Figure 2d**), other bands are also clearly detectable in biomimetic apatites: at lower wavenumbers (attributed to HPO_4 vibrations in either "apatitic" (~550 cm^{-1}) or "non-apatitic" (534 cm^{-1}) chemical environments), and at high wavenumbers (around 617 cm^{-1}, assigned to "non-apatitic" PO_4^{3-} ions). Details of the vibrational spectroscopy features have been reported elsewhere (Rey et al., 2014b) and peak assignments in biomimetic apatites have been specifically discussed in a previous study (Vandecandelaere et al., 2012). While the "apatitic" domains refer to ions located in regular apatite crystallographic sites, "non-apatitic" environments refer to ionic locations that do not correspond to positions within the hydroxyapatite lattice. The latter are located on the surface of the nanocrystals where they are associated with water and form a non-apatitic hydrated ionic layer (Eichert et al., 2005; Rey et al., 2014a).

Therefore, several physicochemical features differ significantly between stoichiometric HAP and nanocrystalline biomimetic apatites: (i) the latter are constituted of nanosized crystals, (ii) they are nonstoichiometric with vacancies in the calcium and hydroxide sites and contain HPO_4^{2-} ions (partly replaced by CO_3^{2-} ions in bone or in synthetic carbonated analogs), (iii) they exhibit an elongated/platelet crystal shape, and (iv) they expose a non-apatitic hydrated ionic layer on their surface. These phenomena represent the four leading conditions defining "biomimetic" or "bone-like" apatite samples. Since these systems are composed of "nano" and "hydrated" crystals, the use of high temperatures (e.g., approaching or beyond the boiling point of the solution), especially for extended periods should be avoided in order to obtain/preserve biomimetic apatite compounds. Consequently, synthesis routes involving at least one wet chemistry step are central.

Hydrated surface layer

As a part of the surface layer, water molecules appear as a key component during crystal genesis. The formation of a hydroxyapatite $Ca_{10}(PO_4)_6(OH)_2$ crystallographic unit cell (hexagonal system, space group $P6_3/m$, Z = 1) involves 44 atoms distributed in the form of 18 ions. Organization of all these ions to elaborate a crystal is thus bound to take time, especially at "low" temperature (e.g., at room or physiological temperature) and under atmospheric pressure. We believe that the hydrated ionic layer on the surface of the nanocrystals might be seen as a "remnant" of the apatite growth process in solution. At neutral/physiological pH, the speciation of phosphate ions clearly favors protonated forms ($HPO_4^{2-}/H_2PO_4^-$) over the deprotonated form PO_4^{3-} which essentially does not exist in these conditions (see phosphoric acid speciation diagram, e.g., Luong et al., 2017). Apatite is however quite insoluble (solubility product ~116 for stoichiometric hydroxyapatite $Ca_{10}(PO_4)_6(OH)_2$, Chander and Fuerstenau, 1984; Elliott, 1994); therefore formation of this calcium phosphate phase can occur even at pHs where only a small amount of phosphate ions PO_4^{3-} is available because the activity product of the ions involved in the apatite precipitation equilibrium (Ca^{2+}, PO_4^{3-}, OH^-) exceeds the solubility product. In (close-to) physiological conditions, it is not surprising that initial phosphate incorporation upon precipitation may involve protonated phosphate ions, and HPO_4^{2-} ions are indeed clearly detected by FTIR especially in surface "non-apatitic" environments (see **Figure 2d**). Some recent papers have introduced the concept of prenucleation clusters involving Ca^{2+} and HPO_4^{2-} ions (Mancardi et al., 2016; Habraken et al., 2013) forming before nucleation. Although experimental evidence for such clusters is difficult to obtain, there is at least a consensus on the strong involvement of protonated phosphate ions at the early stages of apatite nanocrystal formation. In contrast, in the crystal core, deprotonated phosphates become more abundant to approach the HAP composition.

The crystal surface probably cannot be described as a sharp interface between the solid and

the solution (**Figure 3(I)**), but instead as an *interphase* which could be visualized as an extended surface domain progressively allowing the "transition" from the solution to the crystal core as illustrated on **Figure 3(II)**. Solid state NMR data (recorded on dried samples) seem to support this assessment, revealing that the surface layer of moderately mature apatite samples reaches a depth on the nanometer scale (Jager et al., 2006). When apatite nanocrystals are in contact with solution, three components coexist: the solution, the hydrated layer, and the apatite crystal core. The surface layer belongs to the crystal, even after freeze-drying, as shown in Figure 1c/d. This *interphase* involves two "interfaces" (**Figure 3(III)**): a first one between the solution and the hydrated ionic layer, and a second deeper interface between the surface layer and the crystal core itself. 2D solid state NMR (Wang et al., 2012; Rey et al., 2007; Sfihi and Rey, 2002) pointed out correlations through heteronuclear dipolar interaction (for example via $^{1}H \rightarrow ^{31}P$ HetCor experiments), allowing to distinguish RMN-active nuclei that are spatially close to each other. On the one hand, apatitic species like apatitic phosphates and carbonates contained in the crystal core and apatitic OH^- ions correlated with each other. On the other hand, non-apatitic species correlated with each other; indeed non-apatitic (hydrogen)phosphate and labile carbonate species correlated with water molecules. These findings indicate that non-apatitic species are localized in a separate domain as apatitic ones, thus corroborating the "hydrated layer model" already proposed on the basis of vibrational spectroscopy data. It should be emphasized that although XRD data do not provide structural information on the surface layer which is thin and appears "amorphous-like" in the dry state, some degree of organization exists within this layer. Indeed, the spectral signatures of non-apatitic ionic species (e.g., HPO_4^{2-} ions, PO_4^{3-} ions), whether analyzed by FTIR, Raman or NMR, systematically fall at the same positions, suggesting some constancy of chemical environments in synthetic samples and in bone crystals.

The concept of maturation in solution

This surface layer should not be considered as a "simple" hydration layer solely made of water molecules, nor as a Stern electrical double layer, referring to the accumulation of ions and counter-ions from the solution in the form of a double layer on the surface of a solid (Grahame, 1947). Instead, on apatite nanocrystals, this layer contains water closely associated with ions located in chemical environments (**Figure 3(IV)**) that lead to very specific spectroscopic signatures (see for example **Figure 2d**). Upon "maturation", ions gradually fill crystallographic positions corresponding to the apatitic lattice (**Figure 3(IV toVI)**).

The concept of maturation can be investigated experimentally by analyzing apatites left in the precipitating medium for an increasing period of time prior to filtration, washing and (freeze)drying. In carbonate-free conditions, the effect of maturation had been explored in detail (Vandecandelaere et al., 2012). **Figure 4** shows variables of crystal evolution versus the maturation time, quantified by the Ca/P molar ratio of the precipitate, the overall XRD pattern, as well as the mean crystallite dimensions estimated using Scherrer's formula. The physicochemical characteristics of the solid evolve upon aging in solution: (i) the Ca/P ratio increases, indicating an evolution toward HAP stoichiometry (although not reaching it in these conditions), (ii) XRD patterns progressively show increasing crystallinity, and (iii) mean crystallite dimensions systematically increase. These modifications indicate a continuous progression of the crystallization process over the time spent in wet conditions. More in-depth examination of the ionic contents upon maturation also shows that the amount of non-apatitic chemical environments and of overall associated water (followed by TGA) decrease, while the apatitic OH^- content increases (**Figure 5**). These findings indicate that maturation favors the development of the crystalline core at the expense of the surface hydrated ionic layer (**Figure 3(VI)**). It may be noted that the situation is somewhat different in the presence of carbonates: in this case, evolution towards stoichiometry and concomitant increase of OH^-

contents are less noticeable; in contrast a clear increase of carbonation is noticed upon maturation (Eichert, 2001).

It is interesting to examine the maturation process in more detail, by considering the chemical species involved. As indicated above, in the case of carbonate-free samples an increase of the overall Ca/P ratio of the solid phase is observed experimentally. At the atomic/molecular level, this evolution could theoretically be explained either by an increased incorporation of calcium ions in the crystal lattice (increase of numerator), or by a release of phosphate ions (decrease of denominator). However, in physiological or physiological-like conditions corresponding to nanocrystalline apatite precipitation, the amount of free Ca^{2+} ions in solution remains very low (Drouet, 2013) due to the presence of calcium-binding agents such as phosphates, carbonates and proteins. Therefore, the increase of Ca/P may better be explained as a release of phosphate ions expelled from the solid phase during its progression toward stoichiometry (in carbonated conditions CO_3^{2-} ions get progressively incorporated). A proposed overall maturation scheme is represented schematically in **Figure 6**. Both calcium and phosphate ions from the hydrated layer progressively enter the apatitic core. Concerning phosphate, a larger incorporation of PO_4^{3-} ions rather than HPO_4^{2-} is expected in the hydroxyapatite structure; PO_4^{3-} arising from the deprotonation of HPO_4^{2-}, which simultaneously releases protons. Some Ca^{2+} ions are also incorporated to balance electrical charges. Remaining HPO_4^{2-} ions can then combine with the released protons to form monovalent $H_2PO_4^-$ that leaves the crystal, accompanied by the excess of calcium ions. In parallel, a small amount of OH^- can also enter the apatitic core accompanied by calcium ions for preservation of the electroneutrality of the crystal, but this is not represented in **Figure 6** for the sake of simplicity.

The key role of thermodynamics

The chemical evolution undergone by apatite nanocrystals either *in vivo* or in biomimetic analogs appears inevitable as long as apatite nanocrystals are in humid conditions. To explore the thermodynamic basis of this process, oxide melt solution calorimetry has been performed on biomimetic apatites corresponding to increasing maturation times (Rollin-Martinet et al., 2013). These measurements allowed determination of the corresponding standard enthalpy of formation $\Delta H_f°$ of the related apatite compounds via the use of an appropriate thermodynamic cycle. Results, reported in **Table 1**, show that the value of $\Delta H_f°$ for the anhydrous apatite samples (enthalpy of formation from the elements in their standard state, at 298 K and 1 bar) becomes significantly more exothermic upon maturation: enthalpy change is thus associated with the maturation process.

Taking into account entropy estimations (Rollin-Martinet et al., 2013), it also becomes possible to evaluate the corresponding Gibbs free energy of formation $\Delta G_f°$, which is also shown in **Table 1**. Again, a clear trend towards more negative values is seen, with a tendency to evolve towards stoichiometric hydroxyapatite. These results thus indicate that the nanocrystals become increasingly stable as maturation progresses. Comparing the $\Delta G_f°$ values between more and less mature samples allows estimation of the Gibbs free energy accompanying the maturation process, denoted ΔG_{matur} (see below). For this task however, it is necessary also to take into account all the chemical species involved in the maturation process, including participating aqueous ions from the solution (thermodynamic data taken from reference literature sources Robie and Hemingway, 1995 and Wagman et al., 1982). As discussed above and shown schematically in **Figure 6**, maturation is probably accompanied by a release of phosphate rather than an uptake of free Ca^{2+} ions. Considering the following simplified reaction scheme (**Eq. 1**) to describe the change in composition of the apatite phase during maturation:

412

413 *Apatite in initial state* + $\delta_1 H_2O_{(liq)} \rightarrow$ *Apatite in final state* + $\delta_2 H_2PO_4^-{}_{(aq)} + \delta_3 H^+_{(aq)}$ **Eq. 1**

414

415 $\Delta G_{maturation}(i \rightarrow f)$ is given by $\Delta G°_{maturation}(i \rightarrow f) + RT * \ln(K)$ where the equilibrium constant K
416 is the activity product $(H_2PO_4^-{}_{(aq)})^{\delta 2} * (H^+_{(aq)})^{\delta 3}$ (which is close to the corresponding molar
417 concentrations product for sufficiently dilute solutions where activity coefficients are close to
418 1). Taking as initial state the composition of the 20-min matured sample, and considering
419 physiological conditions (pH = 7.4 and $(H_2PO_4^-) \cong 10^{-4}$ M), this leads to negative values of
420 $\Delta G_{maturation}$ (at 298 K), ranging from 0 to -117 ± 23 kJ/mol. The value corresponding to
421 evolution to stoichiometric HAP is -185 ± 15 kJ/mol. Although the effect of carbonation is
422 not taken into account at this stage (thermodynamic data being not available yet for
423 carbonated nanocrystalline apatites), and despite the simplified character of **Eq. 1**, these
424 calculations confirm that H_2O is essential and that maturation is strongly thermodynamically
425 driven and give an order-of-magnitude estimate of the associated energetics.

426 The thermodynamic analysis suggests that immature apatite nanocrystals (e.g., as obtained
427 right after bone remodeling) will inexorably evolve toward more mature compositions as long
428 as they remain in humid conditions. This is not a trivial result as it underlines the fact that
429 even before any "biological" considerations, bone remodeling can be seen as dictated by
430 physical chemistry (thermodynamics) where apatite nanocrystals which have become too
431 mature, stable, and less reactive, have to be dissolved (via osteoclast cells) and re-precipitated
432 (via osteoblast cells) in a renewed immature state. Indeed, bone apatite plays an active role in
433 homeostasis *in vivo* (Driessens et al., 1986), which requires that the high surface reactivity of
434 the constituting nanocrystals (especially via their surface hydrated layer) allow surface ion
435 exchanges to regulate plasma chemical composition, particularly of calcium and phosphate
436 species.

The impact of drying

Interruption of the maturation process can be achieved by separating the solid from the supernatant liquid, which will ultimately require some drying procedure. However, since water molecules are part of the crystal surface, drying is not a trivial task. The object of the present paper is not to examine and compare systematically various drying protocols; it aims, however, to stress the likely modification of the nanocrystal integrity upon such treatments. One way to inspect potential modifications is FTIR spectroscopy, as it is informative about the chemical environment of constitutive chemical species such as phosphates. **Figure 7** reports the analysis of the $\nu_3(PO_4)$ domain, and compares wet and dry states' spectral features for a typical nanocrystalline apatite (matured a few min at 20 °C). A clear deformation of the spectrum can be evidenced upon (freeze)drying: although fine details can be observed on the freshly precipitated sample still wet (very close to the state of well preserved bones, Grunenwald et al., 2014), only a smoothed envelope of vibrational features can be detected for the dried state. This effect suggests further disordering (seen in band broadening) of the surface layer, probably related to the loss of some water. Drying procedures are necessary for the preparation of most bone implants and care should be taken when selecting operating conditions as any (post)treatment of the nanocrystals may affect their intergity and should be examined in detail. This does not preclude the use of nanocrystalline apatite-based systems in medicine, as dried biomimetic apatites were shown to be biologically active and are the closest systems to natural bone. But one must stress that these compounds are hydrated and nanosized and thermodynamically metastable, and therefore they remain potentially sensitive to external treatments, e.g., for material processing, storage or sterilization (Vandecandelaere et al., 2012).

From another angle, for the physical-chemical exploration of nanocrystalline apatites, drying/heating experiments can be envisioned to explore the progressive release of water, e.g.

via TGA (see for example Yoder et al., 2012b). However, it may be remarked that the characteristic temperature of each contribution in thermal analyses is bound to depend upon the conditions of testing; faster heating leading to observation of peak maxima at higher temperature. In addition, importantly for carbonated samples, HPO_4^{2-} ions, if present, may interact with the carbonates during their thermal decomposition by reactions of the type: $2\ HPO_4^{2-} + CO_3^{2-} \rightarrow 2\ PO_4^{3-} + H_2O + CO_2$ leading to significant lowering of the carbonate decomposition temperature, e.g., as low as 250 °C (Legros et al., 1982). Such interactions generate also superimposed effects, which increase the difficulty in accuretely attributing weight losses to specific types of water in cabronated apatites.

Type of associated water molecules

Even after (freeze)drying, apatite nanocrystals remain hydrated. Therefore a question arises as to the type of water molecules remaining in such nanocrystalline apatites. In the present contribution, to investigate this question, differential scanning calorimetry (DSC) measurements were performed, for the first time to our knowledge, on non-carbonated nanocrystalline apatites having undergone increasing maturation times. The samples were heated from -50 to 300 °C at 10 °C/min under a continuous flow of nitrogen. **Figure 8a** reports the typical heat flow signals obtained, with comparison to those of stoichiometric hydroxyapatite (HAP_{st}). For all nanocrystalline apatite samples studied, clear endothermic peaks were seen (not taking into account the small artifact detected around 0 °C assignable to ice residue occurring systematically either on the reference or on the measurement compartment). More precisely, two main wide contributions were detected upon heating, with maxima observed at an average value of 63 °C (336 K) and 113 °C (386 K). In contrast, no such endotherm was detected for stoichiometric HAP (where only a slight endothermic contribution could be seen at higher temperatures, around 200 °C (473 K), due to the

monoclinic → hexagonal phase transition, Suda et al., 1995). The occurrence of these peaks thus appears specific to immature nanocrystalline apatites. Note that TGA data also point to the loss of weight in this temperature range that can reasonably be attributed to water in these non-carbonated samples (Rollin-Martinet et al., 2013), and this weight loss was then used in the thermodynamic study to determine the total amount of water associated with the apatite compounds,.

The endothermic contributions detected here may reasonably be attributed to the water constituting this hydrated interphase, plus the eventual water contained in the apatite structure itself (e.g., in apatite channels or in replacement of the oxygen vacancy left by the CO_3-for-PO_4 substitution), rather than to external/intercrystalline trapped water. Our observations of multiple peaks are similar to DSC data on lyophilized bovine bone, where three endothermic events were observed around 45, 91, and 126 °C (Galia et al., 2011). In that study, the authors tentatively attributed the peak at 45 °C to collagen denaturation and the peak at 91 °C to so-called "water associated with apatite", while the peak at 126 °C was not discussed. Attribution of the 45 °C peak to collagen denaturation however appears questionable as this event generally occurs at higher temperature (Trębacz 2005). If the crystal/collagen interaction involves water, this peak may possibly be linked to alteration of this water at the interface. We believe that the peaks observed at 91 and 126 °C are related to the same origin (water loss) as in the present case on precipitated nanocrystalline apatites. Similarly, two endothermic overlapping events may be seen in the range 20-300 °C on DSC curves reported by Capanema et al. (2015) on niobium-doped precipitated apatite; these events were attributed to "physically adsorbed water" but were not further discussed.

At this stage, it may be remarked that authors should be careful when referring to "adsorbed water" associated with apatite nanocrystals. Care should in particular be taken when dealing with water released well above 200 ° C, which may hardly be assigned to simply "adsorbed",

as documented by Pasteris (2012). Furthermore, the terms "adsorbed water" are probably not the most appropriate to describe the water contained in the hydrated (and ionic) surface layer on apatite nanocrystals; indeed using this terminology may erroneously lead readers to consider it similar to the physisorbed water present on most solid surfaces exposed to moist, while H_2O from the surface layer on apatite nanocrystals is instead closer from compositional water (even if it is not located in the apatitic core of the crystals). The terms "surface water" or "hydrated layer H_2O" should probably be preferred.

Deconvolution of the DSC signals was carried out using the multiple peak fitting tool of the Origin® 8.5 software and considering each (large) contribution as a Gaussian curve, thus allowing us to evaluate the relative proportion of each peak (see an example in **Figure 8b**). **Table 2** reports the results obtained. Considering the "low" temperature of the first endothermic peak, the associated water molecules released may be in a first approximation considered as energetically equivalent to liquid water, as is customary for loosely-bound water. In this case, the energy $\Delta H_1(H_2O)$ required to eliminate one mole of water falls close to 42.5 kJ/mol allowing an estimate of the associated number of moles of water $n_1(H_2O) = \Delta H_{peak\ 1} / \Delta H_1(H_2O)$. Subtracting this value from the total water content determined from TGA then allows evaluation of the number of moles of water associated with peak 2, $n_2(H_2O)$. Finally, it is possible to estimate the energy needed to expel one mole of water in peak 2 (using the C_p of liquid water), giving $\Delta H_2(H_2O) = 48.4 \pm 7.7$ kJ/mol at peak 2 temperature. This corresponds, at 25 °C (298 K), to 52.1 ± 7.7 kJ/mol. This mean value is somewhat larger than the enthalpy of vaporization of water at 298 K (44 kJ/mol), suggesting that this H_2O is indeed somewhat more strongly bound, but the difference is not beyond experimental error.

At least two contributions can thus be evidenced by DSC. The presence of water within the surface layer on the nanocrystals is undeniable as shown in the above and following sections

and recently evidenced again by Wang et al. (2013) by solid state NMR, and release from this surface water is thus expected upon heating. Some authors (e.g., Pasteris et al., 2014, Goldenberg et al., 2015), however, have concluded at least for carbonated systems that a non-negligible amount of water molecules could fill apatite channels. At this stage, it is not possible to distinguish, from these DSC data, which portion of the associated water might be attributed to the surface layer H_2O and which contribution may be related to intracrystalline water.

Upon maturation no clear trend could be identified for $n_1(H_2O)$, reaching a mean around 2 moles H_2O per unit formula (**Figure 9a**). This may be linked, however, to the different "histories" of the freeze-dried samples in contact with the atmosphere for various periods of time. In contrast there is a progressive decrease of $n_2(H_2O)$. The decrease in total water content observed is indeed expected, since the overall hydration of the nanocrystals is experimentally found to decrease with maturation.

In order to inspect the tendency for heated nanocrystalline apatites to partially rehydrate upon contact with moisture, a second DSC run was performed after one week of re-exposure to room atmosphere at ~ 20 °C on a sample (hap-1d) that already had undergone a DSC experiment up to 300 °C (**Figure 9b**). Interestingly, the second run again shows the two clearly detectable peaks at essentially the same temperatures, although with lower intensities. These findings thus show that dehydrated apatite partially rehydrates upon simple re-exposure to water vapor. These observations further support dehydration/partial rehydration data reported by Yoder et al. (2012b). However it is remarkable to note that upon such rehydration, both DSC peaks are affected, indicating that the water related to these two peaks is at least partly reversibly released, which in turn suggests partial "water refilling" of (at least) the surface layer.

These results again point out the key role of water that systematically "associates with"

apatite nanocrystals when they are exposed to a wet environment. The question, however, still remains as to whether intracrystalline water is also present or not in all nanocrystalline apatite samples. For carbonated apatites, several authors agreed on the presence of water in the apatitic lattice, like Ivanova et al. (2001) on the basis of Rietveld refinements of XRD data, or else LeGeros et al. (1978, 1979), Bonel et al. (1975) and Labarthe et al. (1973) on the basis of thermal analyses sometimes assisted by IR analyses, and as reviewed by Pasteris et al. (2014). However, whether this conclusion may be widened to all nanocrystalline apatites including non-carbonated ones is still unclear. There is a lack of direct correlation between the amount of such intracrystalline water and the number of OH vacancies (Pasteris et al., 2014); the amount of H_2O remaining essentially unchanged for all of samples tested in that work. These findings are reminiscent of those obtained in an earlier work by LeGeros et al. (1979) but appear surprising as water molecules, if incorporated in the apatitic channels, would be expected to fill these positions more easily in the case of more OH-deficient samples. However, other parameters such as the co-presence of Na^+ ions might also come into play, although no clear mechanism can yet be formulated precisely. Indeed, the two studies cited above involved sodium ions, while experiments performed in sodium-free conditions led to different results, pointing then to a correlation between the level of carbonation and the total associated water (Labarthe et al., 1973). Also, intracrystalline water might otherwise be located, in carbonated samples, in other positions than apatitic channels, as in the oxygen vacancy left by the substitution of a phosphate by a B-type carbonate group or in calcium vacancies (e.g. Bonel et al. 1975, Ivanova et al., 2001); and water location may even depend on formation conditions. Compositional differences that affect the size of the apatite channels may also affect the amount of intracrystalline water (Goldenberg et al., 2015). In the present DSC study on non-carbonated samples, the re-observation of the two DSC peaks by simple exposure to ambient air seems to favor the hypothesis of surface water refilling rather than a

more internal phenomenon, but additional investigations on various types of nanocrystalline apatite are needed to continue to explore the different locations/types of water molecules, depending on their conditions of formation.

Role of surface water on the spatial organization of apatite nanocrystals

It is interesting at this stage to inspect the role of surface water molecules in the 3D organization of the nanocrystals in a situation where alteration due to drying has been limited as far as possible. In a specific set of experiments, freshly precipitated apatite nanocrystals were left to mature at 25 °C in the mother solution between 1 minute and 1 week, prior to sampling the precipitating medium and analyzing it immediately by cryo-FEG-SEM; the cryogenic mode was selected to limit insofar as possible any alteration of the samples. **Figure 10** shows the typical morphologies obtained. A clear evolution is seen in the course of maturation in solution. At t = 1 min, the precipitate appears as a three dimensional network of spheroid-like particles with a mean diameter around 15 nm, these spheroids tending to organize themselves in pseudo-filaments or relatively linear chains. Progressively, the spheroids evolve toward a more acicular morphology, typically over the first 12 h. At t = 12 h, they have almost totally transformed into a three dimensional arrangement of elongated particles, with a mean length around 50-70 nm and a width close to 10 nm. From then on, the elongated particles are clearly visible and seem to organize in a parallel fashion as “bundles” linked by an amorphous-like domain. At t = 1 week, the particles reach a mean length of about 100 nm and a width of about 7-8 nm and the bundles are still clearly visible. A schematic representation of these morphological modifications is given on **Figure 10**, bottom. It may be noted that the mean size of the spheroids (at t = 1 min) is of the same order as the crystallite dimensions estimated from XRD data and Scherrer’s formula (see **Figure 4c**), suggesting that these spheroids could be individual crystallites. In contrast, for longer

maturation times, the elongated particles exhibit dimensions close to 100 nm which is significantly larger than individual crystallites. We can then assume the formation of polycrystalline particles involving crystallites in strong interaction with each other (aggregation). We have studied the effect of dilution of the precipitation medium on the general aspect of the precipitate, and similar conclusions have been drawn; in particular, bundles of particles were still present but in the form of more separated "islands" dispersed in water. Within each bundle, an amorphous-like domain was still noticed. It may be suggested that the interaction of adjacent nanocrystals via their surface hydrated layers plays a major role in this 3D organization of apatite particles, in particular their tendency to orient in parallel to form bundle-like superstructures. This 3D organization seems to be characteristic of apatite nanocrystals as this has never been reported to our knowledge for well-crystallized hydroxyapatite (which does not exhibit a hydrated layer on its constitutive crystals). This difference may be due to the elongated or flattened morphology of the particles, favoring alignment between most-developed crystal surfaces; but the involvement of the hydrated domains on the nanocrystals, capable of interacting with each other, also appears as a probable hypothesis. The exact mechanism by which adjacent nanocrystals, by way of their hydrated layers, can interact is still unclear. It may involve electrostatic interaction and/or hydrogen bonding between water molecules or HPO_4^{2-} ions; the high mobility of ions within this layer may also help interlacing between two adjacent layers by facilitating diffusive pathways. It may be assumed that a similar scenario of apatite particle alignment should also appear in bone *in vivo*. Wang et al. (2013) have indeed noticed a similar tendency for bone crystals to orient in parallel which is in good agreement with our data on synthetic biomimetic analogs. Such alignment, particularly in a favored direction, may be important in bone repair processes. Indeed, the callus tissue formed upon fracture healing also was found to exhibit preferential crystal orientations (Liu et al., 2010). From another perspective, low gravity

environments in space have been shown to accelerate bone loss. Although bone cell activity was shown to be altered under microgravity (Nabavi et al., 2011), the underlying mechanism is unclear; whether crystal alignment may be influential in the response of bone to microgravity is still unknown.

Consolidation behavior

These findings point out the strong tendency for apatite nanocrystals to interact with each other via their hydrated surface layers. It is thus interesting to investigate the possibility to consolidate these systems into bulk ceramics utilizing this propensity for self-organization. This has been done by way of spark plasma sintering (SPS) at "low" temperature, typically below 300 °C. The first trials of such "cold sintering" having been performed in 2006 (Drouet et al., 2006) and revisited later in detail by Grossin et al. (2010) for hap-1d. Consolidation of nanocrystalline apatite by SPS was shown to be effective. Sintering for 13 min at 150 °C under 100 MPa was found to be the best compromise between a high densification rate and a limitation of nanocrystals alteration. Bulk ceramic pieces were obtained with mechanical properties allowing applications for bone repair. For example, the flexural strength measured from 7 samples of hap-1d by biaxial flexural tests reached 11.3 ± 5.9 MPa. This value is rather high for a material sintered at 150 °C (the non-negligible standard deviation probably results from the defects present in the raw material consolidated by SPS). In contrast, SPS treatment beyond 150 °C led to a delamination phenomenon. We can propose that (i) the consolidation process at such low temperatures is made possible by the presence of interacting surface layers on adjacent nanocrystals allowing easier ion diffusion, and that (ii) the delamination observed at "higher" temperatures is linked to significant dehydration of apatite nanocrystals, altering the surface layer and preventing efficient ion diffusion. This ability for apatite nanocrystals to consolidate appears to be a very peculiar property of these compounds

as they remain noticeably hydrated. This conclusion is also supported in the present work by the consolidation of nanocrystalline apatites having different maturations times, using the same SPS protocol as above (13 min at 150 °C, 100 MPa). However, the relative density of the ceramics noticeably decreased for samples of increasing maturation times (typically from 77 % for hap-20 min down to 53 % for hap-3 weeks). In addition to the small size of the crystals favoring re-orientation under mechanical pressure, the extent of the hydrated layer appears to have a direct effect on their sinterability. The consolidation/sintering of nanocrystalline apatites at "low" temperature may be made possible thanks to the high mobility of ions contained in the hydrated layer. To check surface ion mobility, rapid (few minutes) ion exchange experiments were carried out as previously (Drouet et al., 2008; Eichert et al., 2008). Here, we immersed nanocrystalline apatites in a solution containing Mg^{2+} ions at high concentration (1 M) for 30 min, and followed the replacement of (surface) Ca^{2+} ions by Mg^{2+} by ICP-AES by analyzing the solids before and after ion exchange. **Figure 11** reports the results obtained in terms of "exchangeable" and "non-exchangeable" Ca^{2+} ions. These data show that samples matured for short periods of time exhibit a noticeable amount of exchangeable ions (e.g., up to 8 % of the total Ca^{2+} content), while this amount decreases with maturation time. These results illustrate the high mobility of surface ions from nanocrystalline apatites. In the context of consolidation, as in SPS, this high mobility could allow diffusion phenomena even at "low/moderate" temperatures, while not necessitating strong thermal activation, thus allowing cold sintering. A partial loss of water also appears essential for the consolidation (Grossin et al., 2010), as it allows strong interaction between adjacent crystals.

Extrapolation to the *in vivo* context

Although most of the data given above concern non-carbonated apatites, it is very likely that similar general conclusions can be made for their carbonated counterparts. Indeed,

carbonate ions are known as growth inhibitors for apatite (Sallis, 1998); a carbonated apatite exhibits a more developed hydrated surface layer than its non-carbonated counterpart for the same aging time in solution. *In vivo*, the ion exchange capabilities of apatite nanocrystals represent a way for bone mineral to be active in homeostasis. The natural ability of apatite nanocrystals to align in a parallel way when in wet conditions is likely to occur also *in vivo*, and results from Wang et al. (2013) corroborate this assumption. Like their biomimetic analogs, bone nanocrystals are expected to be thermodynamically metastable, leading to unavoidable evolution toward more stable compositions, closer to stoichiometry. This is probably one non-biological reason for the necessity of bone remodeling, where more mature crystals (becoming less surface-reactive) are progressively dissolved and replaced by new immature, highly reactive nanocrystals.

Implications

All of the above has illustrated the key role of water in the genesis, evolution in solution, 3D particle organization, and general behavior (e.g., via consolidation) of nanocrystalline apatites, whether in bone or in synthetic analogs. The presence of water associated with apatite nanocrystals should therefore not be overlooked, but instead H_2O should be considered as a component of the crystal's composition, at least on its surface. Its elimination, e.g., via drying/heating processes, may fundamentally modify the crystals surface features and reactivity. The surface layer covering the nanocrystals appears as an interphase with potentially gradual properties linking the crystals to the surrounding medium. This hydrated interphase might be seen as a remnant of the apatite growth process in solution. Whether it involves, in early stages, the formation of prenucleation clusters is still undetermined. In any case the apatite and its hydrated layer should be considered, in our opinion, as appearing simultaneously. Intermediate metastable phases, e.g., amorphous calcium phosphate or

712 "ACP", may transiently be formed in the precipitating medium, depending on the apatite
713 formation conditions. ACP is likely involved for example in the preparation of synthetic
714 analogs where concentrations/supersaturation are generally higher than *in vivo*; and apatite
715 may then crystallize from the amorphous phase. A question can then arise as whether the
716 formation and evolution/growth of apatite nuclei within this ACP might structure the crystal
717 and its surface layer, but this is still under study. Another phenomenon should also be
718 considered when dealing with the formation of apatite from an amorphous phase without
719 changing the Ca/P ratio: the internal hydrolysis of PO_4^{3-} ions. In this process, the
720 simultaneous formation of OH^- and HPO_4^{2-} ions arises from reaction of water with PO_4^{3-} ions.
721 It is not clear however whether this reaction occurs in bone or not. IR and Raman
722 spectroscopies only point to limited amounts of OH^- even for mature bone (e.g. Pasteris et al.,
723 2004; Rey et al., 1995). NMR seems in contrast to identify larger hydroxide contents (e.g.
724 Cho et al., 2003), but this internal hydrolysis reaction might explain the relative divergence
725 between vibrational spectroscopies and NMR, taking into account the fact that NMR
726 generates some sample heating and necessitates longer acquisition times than Raman or IR.

727 The location of water molecules in bone apatite nanocrystals and biomimetic analogs is still
728 being debated and explored. The presence of water within the surface layer on the
729 nanocrystals is obvious, but additional water is also reported for carbonated apatites to be
730 trapped in the structure although incorporation mechanisms have still to be clarified. As a
731 perspective, additional exploration of the water environments within the surface layer and
732 inside the structure is needed to better comprehend biomineralization phenomena as well as
733 biomimetic apatite-based biomaterials processing. In addition, methods should be further
734 developed for quantifying the relative volume of the hydrated layer covering apatite
735 nanocrystals, and the relative amounts of water in the various reservoirs associated with
736 nanocrystalline apatites.

737

738 **Acknowledgements:**

739 The authors thank the *Agence Nationale de la Recherche* (ANR) for funding in the scope of
740 the *NanoBiocer* and *BioCapabili* projects (ANR-07-BLAN-0373 and PICF 2009). The
741 thermodynamic work at Davis was supported by the France Berkeley Fund (FBF) and the
742 Institut National Polytechnique de Toulouse (INPT).

743 The authors also thank the GdR CNRS n°3584 *TherMatHT* (www.thermatht.fr) and the
744 *Thermodynamics Consortium* (www.thermocon.org) for fruitful discussion and collaborative
745 work on the present contribution.

746

747 **References:**

748

749 Bonel, G., Labarthe, J.C., and Vignoles, C. (1975) Contribution à l'étude structurale des
750 apatites carbonatées de type B. In CNRS, Ed., Physico-Chimie et Cristallographie des
751 Apatites d'intérêt Biologique, p. 117-125. Colloques Internationaux du Centre
752 National de la Recherche Scientifique, Paris.

753 Bonjour, J.P. (2011) Calcium and Phosphate: A Duet of Ions Playing for Bone Health. Journal
754 of the American College of Nutrition, 30, 438S-448S.

755 Bouladjine, A., Al-Kattan, A., Dufour, P., and Drouet, C. (2009) New Advances in
756 Nanocrystalline Apatite Colloids Intended for Cellular Drug Delivery. Langmuir, 25,
757 12256-12265.

758 Capanema, N.S.V., Mansur, A.A.P., Carvalho, S.M., Silva, A.R.P., Ciminelli, V.S., and
759 Mansur, H.S. (2015) Niobium-Doped Hydroxyapatite Bioceramics: Synthesis,
760 Characterization and In Vitro Cytocompatibility. Materials, 8, 4191-4209.

761 Carlström, D., Glas, J.E., and Angmar, B. (1963) Studies on the ultrastructure of dental
762 enamel: V. The state of water in human enamel. Journal of Ultrastructure Research, 8,
763 24-29.

764 Cazalbou, S., Combes, C., Eichert, D., Rey, C., and Glimcher, M.J. (2004a) Poorly crystalline
765 apatites: evolution and maturation in vitro and in vivo. Journal of Bone and Mineral
766 Metabolism, 22, 310-317.

767 Cazalbou, S., Eichert, D., Drouet, C., Combes, C., and Rey, C. (2004b) Biological
768 mineralisations based on calcium phosphate. Comptes Rendus Palevol, 3, 563-572.

769 Chander, S, and Fuerstenau, D.W. (1984) Solubility and interfacial properties of
770 hydroxyapatite: a review. In D.N. Misra, Ed., Adsorption on and Surface
771 Chemistry of Hydroxyapatite, p. 29-49. Plenum Press, New York.

772 Cho, G., Wu, Y., and Ackerman, J. L. (2003) Detection of hydroxyl ions in bone mineral by
773 solid-state NMR spectroscopy. Science, 300, 1123-1127.
774 Chowdhury, E.H., and Akaike, T. (2005) Advances in fabrication of calcium phosphate nano-
775 composites for smart delivery of DNA and RNA to mammalian cells. Current
776 Analytical Chemistry, 1, 187-192.
777 Delgado-Lopez, J.M., Iafisco, M., Rodriguez, I., Tampieri, A., Prat, M., and Gomez-Morales,
778 J. (2012) Crystallization of bioinspired citrate-functionalized nanoapatite with tailored
779 carbonate content. Acta Biomaterialia, 8, 3491-3499.
780 Della Gatta, G., Richardson Michael, J., Sarge Stefan, M., and Stølen, S. (2006) Standards,
781 calibration, and guidelines in microcalorimetry. Part 2. Calibration standards for
782 differential scanning calorimetry (IUPAC Technical Report). Pure and Applied
783 Chemistry, 78, 1455.
784 Driessens, F.C.M., Vandijk, J.W.E., and Verbeeck, R.M.H. (1986) The role of bone-mineral
785 in calcium and phosphate homeostasis. Bulletin Des Societes Chimiques Belges, 95,
786 337-342.
787 Drouet, C. (2013) Apatite Formation: Why It May Not Work as Planned, and How to
788 Conclusively Identify Apatite Compounds. Biomed Research International, 2013,
789 Article ID 490946, 1-12.
790 Drouet, C., Al-Kattan, A., Choimet, M., Tourrette, A., Santran, V., Dexpert-Ghys, J., Pipy, B.,
791 Brouillet, F., and Tourbin, M. (2015) Biomimetic Apatite-Based Functional
792 Nanoparticles as Promising Newcomers in Nanomedicine: Overview of 10 Years of
793 Initiatory Research. Journal of General Practice and Medical Diagnosis (GPMD), 1, 1-
794 9.

795 Drouet, C., Bosc, F., Banu, M., Largeot, C., Combes, C., Dechambre, G., Estournès, C.,
796 Raimbeaux, G., and Rey, C. (2009) Nanocrystalline apatites: From powders to
797 biomaterials. Powder Technology, 190, 118-122.
798 Drouet, C., Carayon, M.-T., Combes, C., and Rey, C. (2008) Surface enrichment of
799 biomimetic apatites with biologically-active ions Mg^{2+} and Sr^{2+}: A preamble to the
800 activation of bone repair materials. Materials Science and Engineering C, 28, 1544-
801 1550.
802 Drouet, C., Largeot, C., Raimbeaux, G., Estournes, C., Dechambre, G., Combes, C., and Rey,
803 C. (2006) Bioceramics: spark plasma sintering (SPS) of calcium phosphates. Adv. Sci.
804 Technol., 49, 45-50.
805 Eichert, D. (2001) Etude de la reactivite de surface d'apatites de synthese nanocristallines,
806 PhD Thesis. Institut National Polytechnique de Toulouse, Toulouse, France.
807 Eichert, D., Combes, C., Drouet, C., and Rey, C. (2005) Formation and evolution of hydrated
808 surface layers of apatites. Key Engineering Materials, 284-286, 3-6.
809 Eichert, D., Drouet, C., Sfihi, H., Rey, C., and Combes, C. (2007) Nanocrystalline apatite
810 based biomaterials: synthesis, processing and characterization. In J.B. Kendall, Ed.,
811 Biomaterials Research Advances, p. 93-143. Nova Science Publishers, New York.
812 Elliott, J.C. (1994) Structure and Chemistry of the Apatites and Other Calcium
813 Orthophosphates, 389 p. Elsevier, Amsterdam.
814 Galia, C.R., Lourenço, A.L., Rosito, R., Macedo, C.A.S., and Camargo, L.M.A.Q. (2011)
815 Caracterização físico-química do enxerto de osso bovino liofilizado. Revista Brasileira
816 de Ortopedia, 46, 444-451.
817 Glimcher, M.J. (1959) Molecular Biology of Mineralized Tissues with Particular Reference to
818 Bone. Reviews of Modern Physics, 31, 359-393.

819 Goldenberg, J.E., Wilt, Z., Schermerhorn, D.V., Pasteris, J.D., and Yoder, C.H. (2015)
820 Structural effects on incorporated water in carbonated apatites. American
821 Mineralogist, 100, 274-280.
822 Gomez-Morales, J., Iafisco, M., Manuel Delgado-Lopez, J., Sarda, S., and Drouet, C. (2013)
823 Progress on the preparation of nanocrystalline apatites and surface characterization:
824 Overview of fundamental and applied aspects. Progress in Crystal Growth and
825 Characterization of Materials, 59, 1-46.
826 Grahame, D.C. (1947) The Electrical Double Layer and the Theory of Electrocapillarity.
827 Chemical Reviews, 41, 441-501.
828 Granke, M., Does, M.D., and Nyman, J.S. (2015) The Role of Water Compartments in the
829 Material Properties of Cortical Bone. Calcified tissue international, 97, 292-307.
830 Grossin, D., Rollin-Martinet, S., Estournes, C., Rossignol, F., Champion, E., Combes, C.,
831 Rey, C., Chevallier, G., and Drouet, C. (2010) Biomimetic apatite sintered at very low
832 temperature by spark plasma sintering: Physico-chemistry and microstructure aspects.
833 Acta Biomaterialia, 6, 577-585.
834 Grunenwald, A., Keyser, C., Sautereau, A.M., Crubezy, E., Ludes, B., and Drouet, C. (2014)
835 Novel contribution on the diagenetic physicochemical features of bone and teeth
836 minerals, as substrates for ancient DNA typing. Analytical and Bioanalytical
837 Chemistry, 406, 4691-4704.
838 Grynpas, M. (1976) Crystallinity of bone-mineral. Journal of Materials Science, 11, 1691-
839 1696.
840 Habraken, W.J., Tao, J., Brylka, L.J., Friedrich, H., Bertinetti, L., Schenk, A.S., Verch, A.,
841 Dmitrovic, V., Bomans, P.H., Frederik, P.M., Laven, J., van der Schoot, P.,
842 Aichmayer, B., de With, G., DeYoreo, J.J., and Sommerdijk, N.A. (2013) Ion-

association complexes unite classical and non-classical theories for the biomimetic nucleation of calcium phosphate. Nat Commun, 4, article #1507, 1-12.

Hossain, S., Stanislaus, A., Chua, M.J., Tada, S., Tagawa, Y.-i., Chowdhury, E.H., and Akaike, T. (2010) Carbonate apatite-facilitated intracellularly delivered siRNA for efficient knockdown of functional genes. Journal of Controlled Release, 147, 101-108.

Iafisco, M., Delgado-Lopez, J.M., Gomez-Morales, J., Hernandez-Hernandez, M.A., Rodriguez-Ruiz, I., and Roveri, N. (2011) Formation of calcium phosphates by vapour diffusion in highly concentrated ionic micro-droplets. Crystal Research and Technology, 46, 841-846.

Iafisco, M., Manuel Delgado-Lopez, J., Varoni, E.M., Tampieri, A., Rimondini, L., Gomez-Morales, J., and Prat, M. (2013) Cell Surface Receptor Targeted Biomimetic Apatite Nanocrystals for Cancer Therapy. Small, 9, 3834-3844.

Iafisco, M., Palazzo, B., Martra, G., Margiotta, N., Piccinonna, S., Natile, G., Gandin, V., Marzano, C., and Roveri, N. (2012) Nanocrystalline carbonate-apatites: role of Ca/P ratio on the upload and release of anticancer platinum bisphosphonates. Nanoscale, 4, 206-217.

Ivanova, T. I., Frank-Kamenetskaya, O. V., Kol'tsov, A. B., and Ugolkov, V. L. (2001) Crystal Structure of Calcium-Deficient Carbonated Hydroxyapatite. Thermal Decomposition. Journal of Solid State Chemistry, 160, 340-349.

Jäger, C., Welzel, T., Meyer-Zaika, W., and Epple, M. (2006) A solid-state NMR investigation of the structure of nanocrystalline hydroxyapatite. Magnetic Resonance in Chemistry, 44, 573-580.

Kaflak, A., and Kolodziejski, W. (2008) Kinetics H-1 -> P-31 NMR cross-polarization in bone apatite and its mineral standards. Magnetic Resonance in Chemistry, 46, 335-341.

868 Kramer, E., Itzkowitz, E., and Wei, M. (2014) Synthesis and characterization of cobalt-
869 substituted hydroxyapatite powders. Ceramics International, 40, 13471-13480.
870 Labarthe, J.C., Bonel, G., and Montel, G. (1973) Sur la structure et les propriétés des apatites
871 carbonatées de type B phosphocalciques, Ann. Chim. 8, 289-301.
872 LeGeros, R.Z., Bonel, G., and Legros, R. (1978) Types of H_2O in human enamel and in
873 precipitated apatites. Calcified Tissue Research, 26, 111-118.
874 LeGeros, R.Z., Legros, R., and Bonel, G. (1979) Sur la déshydratation des apatites
875 carbonatées de type B sodées. C. R. Acad. Sc. Paris, 288 C, 81-84
876 LeGeros, R.Z., and LeGeros, J.P. (1984) Phosphate Minerals in Human Tissues. In J.O.
877 Nriagu, and P.B. Moore, Eds., Phosphate Minerals, p. 351-385. Springer, Heidelberg,
878 Berlin.
879 Legros R., Balmain N., and Bonel G. (1987) Age-related changes in mineral of rat and bovine
880 cortical bone. Calcif. Tissue Int., 41, 137-144.
881 Legros, R., Godinot, C., Torres, L., Mathieu, J., and Bonel, G. (1982) Sur la stabilité
882 thermique des carbonates du tissu osseux, Journal de Biologie Buccale, 10, 3-9.
883 Liu, Y., Manjubala, I., Roschger, P., Schell, H., Duda, G.N., and Peter Fratzl (2010) Mineral
884 crystal alignment in mineralized fracture callus determined by 3D small-angle X-ray
885 scattering. Journal of Physics: Conference Series, 247, 012031.
886 Lu, H.B., Campbell, C.T., Graham, D.J., and Ratner, B.D. (2000) Surface characterization of
887 hydroxyapatite and related calcium phosphates by XPS and TOF-SIMS. Analytical
888 Chemistry, 72, 2886-2894.
889 Luong H. V. T., and Liu J. C. (2017) Flotation separation of strontium via phosphate
890 precipitation. Water Science and Technology,75, 2520-2526.

Mancardi, G., Terranova, U., and de Leeuw, N.H. (2016) Calcium Phosphate Prenucleation Complexes in Water by Means of ab Initio Molecular Dynamics Simulations. Crystal Growth & Design, 16, 3353-3358.

Nabavi, N., Khandani, A., Camirand, A., and Harrison, R. E. (2011) Effects of microgravity on osteoclast bone resorption and osteoblast cytoskeletal organization and adhesion. Bone 49, 965-74.

Neuman, W.F., and Neuman, M.W. (1953a) The Nature of the Mineral Phase of Bone. Chemical Reviews, 53, 1-45.

Neuman, W.F., Toribara, T.Y., and Mulryan, B.J. (1953b) The Surface Chemistry of Bone. VII. The Hydration Shell1. Journal of the American Chemical Society, 75, 4239-4242.

Nyman, J.S., Ni, Q., Nicolella, D.P., and Wang, X. (2008) Measurements of mobile and bound water by nuclear magnetic resonance correlate with mechanical properties of bone. Bone, 42, 193-9.

Nyman, J.S., Roy, A., Shen, X., Acuna, R.L., Tyler, J.H., and Wang, X. (2006) The influence of water removal on the strength and toughness of cortical bone. Journal of biomechanics, 39, 931-938.

Pasteris, J. D., Yoder, C.H., and Wopenka, B. (2014) Molecular water in nominally unhydrated carbonated hydroxylapatite: The key to a better understanding of bone mineral. American Mineralogist, 99, 16-27.

Pasteris, J.D. (2012) Structurally incorporated water in bone apatite: A cautionary tale. In R.B. Heimann, Ed., Calcium Phosphates: Structure, Synthesis, Properties, and Applications, p. 63-94. Nova Science Publishers, New York.

Pasteris, J. D., Yoder, C.H., Sterlieb, M.P., and Liu, S. (2012) Effect of carbonate incorporation on the hydroxyl content of hydroxylapatite. Mineralogiscal Magazine 76, 2741-2759.

916 Pasteris, J. D., Wopenka, B., Freeman, J. J., Rogers, K., Valsami-Jones, E., van der Houwen,
917 J. A. M., and Silva, M. J. (2004) Lack of OH in nanocrystalline apatite as a function of
918 degree of atomic order: implications for bone and biomaterials. Biomaterials, 25, 229-
919 238.
920 Raynaud, S., Champion, E., Bernache-Assollant, D., and Thomas, P. (2002) Calcium
921 phosphate apatites with variable Ca/P atomic ratio I. Synthesis, characterisation and
922 thermal stability of powders. Biomaterials, 23, 1065-1072.
923 Rey, C., Combes, C., Drouet, C., Cazalbou, S., Grossin, D., Brouillet, F., and Sarda, S.
924 (2014a) Surface properties of biomimetic nanocrystalline apatites; applications in
925 biomaterials. Progress in Crystal Growth and Characterization of Materials, 60, 63-73.
926 Rey, C., Combes, C., Drouet, C., and Glimcher, M. (2009) Bone mineral: update on chemical
927 composition and structure. Osteoporosis International, 20, 1013–1021.
928 Rey, C., Combes, C., Drouet, C., Sfihi, H., and Barroug, A. (2007) Physico-chemical
929 properties of nanocrystalline apatites: Implications for biominerals and biomaterials.
930 Materials Science and engineering C, 27, 198-205.
931 Rey, C., Lian, J., Grynpas, M., Shapiro, F., Zylberberg, L., and Glimcher, M.J. (1989) Non-
932 apatitic environments in bone mineral: FT-IR detection, biological properties and
933 changes in several disease states. Connective tissue research, 21, 267-73.
934 Rey, C., Marsan, O., Combes, C., Drouet, C., Grossin, D., and Sarda, S. (2014b)
935 Characterization of Calcium Phosphates Using Vibrational Spectroscopies. In B. Ben-
936 Nissan, Ed., Advances in Calcium Phosphate Biomaterials, 2, p. 229-266. Springer,
937 Berlin Heidelberg,.
938 Rey, C., Miquel, J. L., Facchini, L., Legrand, A. P., and Glimcher, M. J. (1995) Hydroxyl
939 groups in bone mineral. Bone, 16, 583-586.

940 Rey, C., Shimizu, M., Collins, B., and Glimcher, M.J. (1990) Resolution-enhanced Fourier-
941 transform infrared-spectroscopy study of the environment of phosphate ions in the
942 early deposits of a solid-phase of calcium-phosphate in bone and enamel, and their
943 evolution with age. 1. Investigations in the ν_4PO_4 domain. Calcified Tissue
944 International, 46, 384-394.
945 Robie, R.A., and Hemingway, B.S. (1995) U.S. Geological Survey Bull., 2131.
946 Rollin-Martinet, S. (2011) Developpement de nouvelles bioceramiques par consolidation a
947 basse temperature d'apatites nanocristallines biomimetiques. PhD, Université de
948 Limoges, France.
949 Rollin-Martinet, S., Navrotsky, A., Champion, E., Grossin, D., and Drouet, C. (2013)
950 Thermodynamic basis for evolution of apatite in calcified tissues. American
951 Mineralogist, 98, 2037-2045.
952 Roufosse, A.H., Aue, W.P., Roberts, J.E., Glimcher, M.J., and Griffin, R.G. (1984)
953 Investigation of the mineral phases of bone by solid-state P-31 magic angle sample
954 spinning nuclear magnetic-resonance. Biochemistry, 23, 6115-6120.
955 Sallis, J. D. (1998) Structure/Performance Relationships of Phosphorous and Carboxyl
956 Containing Additives as Calcium Phosphate Crystal Growth Inhibitors. In Z. Amjad,
957 Ed., Calcium Phosphates in Biological and Industrial Systems, p. 173–191. Kluwer
958 Academic, Dordrecht.
959 Sfihi, H., and Rey, C. (2002) 1-D and 2-D Double Heteronuclear Magnetic Resonance Study
960 of the Local Structure of Type B Carbonate Fluoroapatite. In J. Fraissard, and O.
961 Lapina, Eds., Magnetic Resonance in Colloid and Interface Science, p. 409-422.
962 Springer Netherlands, Dordrecht.
963 Sokolova, V.V., Radtke, I., Heumann, R., and Epple, M. (2006) Effective transfection of cells
964 with multi-shell calcium phosphate-DNA nanoparticles. Biomaterials, 27, 3147-3153.

965 Stefanic, M., Ward, K., Tawfik, H., Seemann, R., Baulin, V., Guo, Y., Fleury, J.-B., and
966 Drouet, C. (2017) Apatite nanoparticles strongly improve red blood cell
967 cryopreservation by mediating trehalose delivery via enhanced membrane permeation.
968 Biomaterials, 140, 138-149.
969 Suda, H., Yashima, M., Kakihana, M., and Yoshimura, M. (1995) Monoclinic .tautm.
970 Hexagonal Phase Transition in Hydroxyapatite Studied by X-ray Powder Diffraction
971 and Differential Scanning Calorimeter Techniques. The Journal of Physical
972 Chemistry, 99, 6752-6754.
973 Timmins, P.A., and Wall, J.C. (1977) Bone water. Calcif Tissue Res, 23, 1-5.
974 Trębacz, H., and Wójtowicz, K. (2005) Thermal stabilization of collagen molecules in bone
975 tissue. International Journal of Biological Macromolecules, 37, 257-262.
976 Unal, M., and Akkus, O. (2015) Raman spectral classification of mineral- and collagen-bound
977 water's associations to elastic and post-yield mechanical properties of cortical bone.
978 Bone, 81, 315-26.
979 Ushakov, S.V., Helean, K.B., Navrotsky, A., and Boatner, L.A. (2001) Thermochemistry of
980 rare-earth orthophosphates. Journal of Materials Research, 16, 2623-2633.
981 Vandecandelaere, N., Rey, C., and Drouet, C. (2012) Biomimetic apatite-based biomaterials:
982 on the critical impact of synthesis and post-synthesis parameters. Journal of Materials
983 Science-Materials in Medicine, 23, 2593-2606.
984 Wagman, D.D., Evans, W.H., Parker, V.B., Schumm, R.H., Halow, I., Bailey, S.M., Churney,
985 K.L., and Nuttall, R.L. (1982) The NBS tables of chemical thermodynamic properties
986 – Selected values for inorganic and C-1 and C-2 organic-substances in SI units.
987 Journal of Physical and Chemical Reference Data, 11, 1-&.
988 Wang, Y., Azais, T., Robin, M., Vallee, A., Catania, C., Legriel, P., Pehau-Arnaudet, G.,
989 Babonneau, F., Giraud-Guille, M.M., and Nassif, N. (2012) The predominant role of

collagen in the nucleation, growth, structure and orientation of bone apatite. Nat Mater, 11, 724-33.

Wang, Y., Von Euw, S., Fernandes, F.M., Cassaignon, S., Selmane, M., Laurent, G., Pehau-Arnaudet, G., Coelho, C., Bonhomme-Coury, L., Giraud-Guille, M.-M., Babonneau, F., Azaïs, T., and Nassif, N. (2013) Water-mediated structuring of bone apatite. Nat Mater, 12, 1144-1153.

Wilson, E. E., Awonusi, A., Morris, M. D., Kohn, D. H., Tecklenburg, M. M. J., and Beck, L. W. (2006) Three Structural Roles for Water in Bone Observed by Solid-State NMR. Biophysical Journal, 90, 3722-3731.

Wilson, E. E., Awonusi, A., Morris, M. D., Kohn, D. H., Tecklenburg, M. M., and Beck, L. W. (2005) Highly ordered interstitial water observed in bone by nuclear magnetic resonance. J Bone Miner Res, 20, 625-34.

Yoder, C. H., Pasteris, J. D., Worcester, K. N., and Schermerhorn, D. V. (2012a) Structural water in carbonated hydroxylapatite and fluorapatite: confirmation by solid state (2)H NMR. Calcif Tissue Int, 90, 60-67.

Yoder, C., Pasteris, J., Worcester, K., Schermerhorn, D., Sternlieb, M., Goldenberg, J., and Wilt, Z. (2012b) Dehydration and rehydration of carbonated fluor- and hydroxylapatite, Minerals, 2, 100-117.

Table captions:

Table 1: Experimental ΔH_{ds} values and derived $\Delta H_{f,oxides}$, $\Delta H_f°$ and $\Delta G_f°$ for nanocrystalline apatites with increasing maturation states

Table 2: DSC data for nanocrystalline apatites corresponding to increasing maturation times

Figure captions:

Figure 1: Possible position of vacancies in the apatite lattice, where some water molecules could potentially reside (beside the water contained within the surface hydrated layer on the nanocrystals): a) vacancies in OH- (on the axis of apatitic channels) and Ca2+ sites (CaI and CaII) represented on the basis of the hydroxyapatite crystal lattice, b) oxygen vacancy left in the case of CO3-for-PO4 substitution (B-type carbonate). In this schematic representation, no distortion of the PO4 tetrahedron nor of the CO3 plane are shown.

Figure 2: Typical characteristics of biomimetic nanocrystalline apatites (e.g. matured 1 day (a,b,c) or 3 weeks (d)) and of stoichiometric HAP sintered at 1000 °C-1 h (b,c). a) TEM micrograph, b) XRD pattern (λ_{cobalt} = 1.78892 Å), c) FTIR spectra and d) detail on the $\nu_4(PO_4)$ FTIR spectral domain

Figure 3: Schematic representation of an apatite nanocrystal in contact with an aqueous medium (carbonate free conditions)

Figure 4: Effect of apatite maturation in solution (at 22 °C) on (a) Ca/P molar ratio, (b) XRD pattern (λ_{copper} = 1.514 Å), and (c) mean crystallite dimensions as estimated from Scherrer's formula

Figure 5: Evolution of ionic contents of nanocrystalline apatites versus maturation (at 22 °C): (a) Ca^{2+} and OH^- contents per unit formula and (b) example of H_2O content per unit formula (as measured from TGA for one given set of batches freeze-dried for 3 days) and evolution of non-apatitic HPO_4^{2-} environments (in relative proportion from FTIR analysis of the $\nu_4(PO_4)$ band: peak area ratio between n.ap. HPO_4 band at 534 cm^{-1} and overall $\nu_4(PO_4)$ band area)

Figure 6: General scheme for apatite maturation in solution (carbonate free conditions)

Figure 7: Effect of drying on the $\nu_3(PO_4)$ domain as followed by FTIR spectroscopy for a nanocrystalline apatite sample matured few min at 20 °C

Figure 8: : a) DSC signal upon heating (at 10 °C/min) nanocrystalline apatites from -50 up to 300 °C under nitrogen flow, for various maturation times. Curves have been shifted intentionally for facilitating the reading. b) Example of deconvolution of DSC signal for hap-1 day

Figure 9: Evolution of $n_1(H_2O)$ and $n_2(H_2O)$ as evaluated from DSC data: a) for samples with increasing maturation times and b) effect of re-exposure to atmosphere on sample hap-1d

Figure 10: Cryo-FEG-SEM observations of nanocrystalline apatites matured at 25 °C between 1 min and 1 week and directly analyzed (initial magnification: x 150 000), and schematic representation of the evolutional change of morphology

Figure 11: Evolution of exchangeable Ca^{2+} ions by Mg^{2+} by surface ion exchanges, for apatites with increasing maturation times

This is a preprint, the final version is subject to change, of the American Mineralogist (MSA)
Cite as Authors (Year) Title. American Mineralogist, in press.
DOI: https://doi.org/10.2138/am-2018-6415

Table 1: Experimental ΔH_{ds} values and derived $\Delta H_{f,oxides}$, $\Delta H_f°$ and $\Delta G_f°$ for nanocrystalline apatites with increasing maturation states

Sample	ΔH_{ds} (apatite, hydrated) (kJ/mol)	$\Delta H_f°$ (apatite, hydrated) (kJ/mol)	$\Delta H_{f\,oxides}$ (kJ/mol)	**$\Delta H_f°$ (apatites, anhydrous) (kJ/mol)**	**$\Delta G°_f$ kJ/mol**
Nanocrystalline apatites:					
20 min	1197.7 ± 10.0 (10)	-13756.8 ± 12.2	-1952.2 ± 12.5	**-12058.9 ± 12.2**	**-11323.1 ± 12.2**
3 hour	1198.2 ± 15.0 (9)	-13370.7 ± 16.5	-2073.9 ± 16.8	**-12174.9 ± 16.5**	**-11439.7 ± 16.5**
1 day	1241.7 ± 9.5 (8)	-13393.4 ± 11.8	-2152.7 ± 12.1	**-12364.4 ± 11.8**	**-11616.0 ± 11.8**
3 days	1088.6 ± 9.1 (9)	-13352.3 ± 11.5	-2032.8 ± 11.8	**-12342.1 ± 11.5**	**-11595.0 ± 11.5**
5 days	1077.4 ± 5.1 (9)	-13373.3 ± 8.7	-2030.5 ± 9.2	**-12457.0 ± 8.7**	**-11692.6 ± 8.7**
1 week	1137.2 ± 9.1 (10)	-13362.2 ± 11.5	-2119.5 ± 11.9	**-12546.1 ± 11.5**	**-11783.9 ± 11.5**
3 weeks	1172.8 ± 20.2 (9)	-13708.7 ± 21.4	-2141.3 ± 21.6	**-12771.0 ± 21.4**	**-11994.2 ± 21.4**
HAP st.	1027.7 ± 21.4 (11)	-13477 ± 10	-2283.5 ± 23.0	**-13477 ± 10**	**-12674.2 ± 10**

* numbers in parentheses refer to the number of calorimetry experiments performed

Table 2: DSC data for nanocrystalline apatites corresponding to increasing maturation times

Maturation time	ΔH_{total} (kJ/mol)	$\Delta H_{peak\ 1}$ (kJ/mol)	$\Delta H_{peak\ 2}$ (kJ/mol)	$n_1(H_2O)$ from peak 1 per mole of apatite	$n_2(H_2O)$ from peak 2 per mole of apatite
20 min	176	88	88	2.1	1.8
3 h	178	110	68	2.6	1.4
1 d	143	72	72	1.7	1.5
3 d	169	90	78	2.1	1.6
5 d	147	70	76	1.7	1.6
1 w	137	80	57	1.9	1.2
3 w	143	95	47	2.3	1.0
1 d re-exposed	92	45	47	1.1	1.0

This is a preprint, the final version is subject to change, of the American Mineralogist (MSA)
Cite as Authors (Year) Title. American Mineralogist, in press.
DOI: https://doi.org/10.2138/am-2018-6415

Figure 1: Possible position of vacancies in the apatite lattice, where some water molecules could potentially reside (beside the water contained within the surface hydrated layer on the nanocrystals): a) vacancies in OH^- (on the axis of apatitic channels) and Ca^{2+} sites (Ca_I and Ca_{II}) represented on the basis of the hydroxyapatite crystal lattice, b) oxygen vacancy left in the case of CO_3-for-PO_4 substitution (B-type carbonate). In this schematic representation, no distortion of the PO_4 tetrahedron nor of the CO_3 plane are shown.

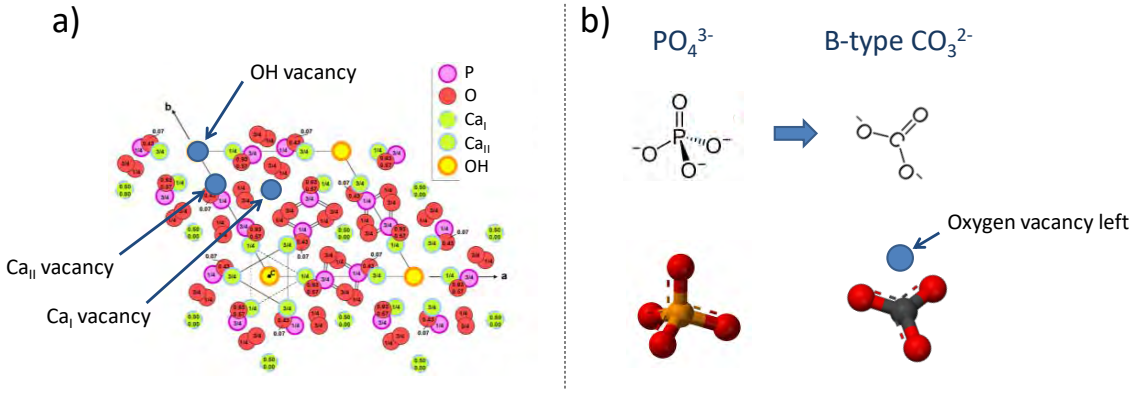

This is a preprint, the final version is subject to change, of the American Mineralogist (MSA)
Cite as Authors (Year) Title. American Mineralogist, in press.
DOI: https://doi.org/10.2138/am-2018-6415

Figure 2: Typical characteristics of biomimetic nanocrystalline apatites (e.g. matured 1 day (a,b,c) or 3 weeks (d)) and of stoichiometric HAP sintered at 1000 °C-1 h (b,c). a) TEM micrograph, b) XRD pattern (λ_{cobalt} = 1.78892 Å), c) FTIR spectra and d) detail on the $\nu_4(PO_4)$ FTIR spectral domain

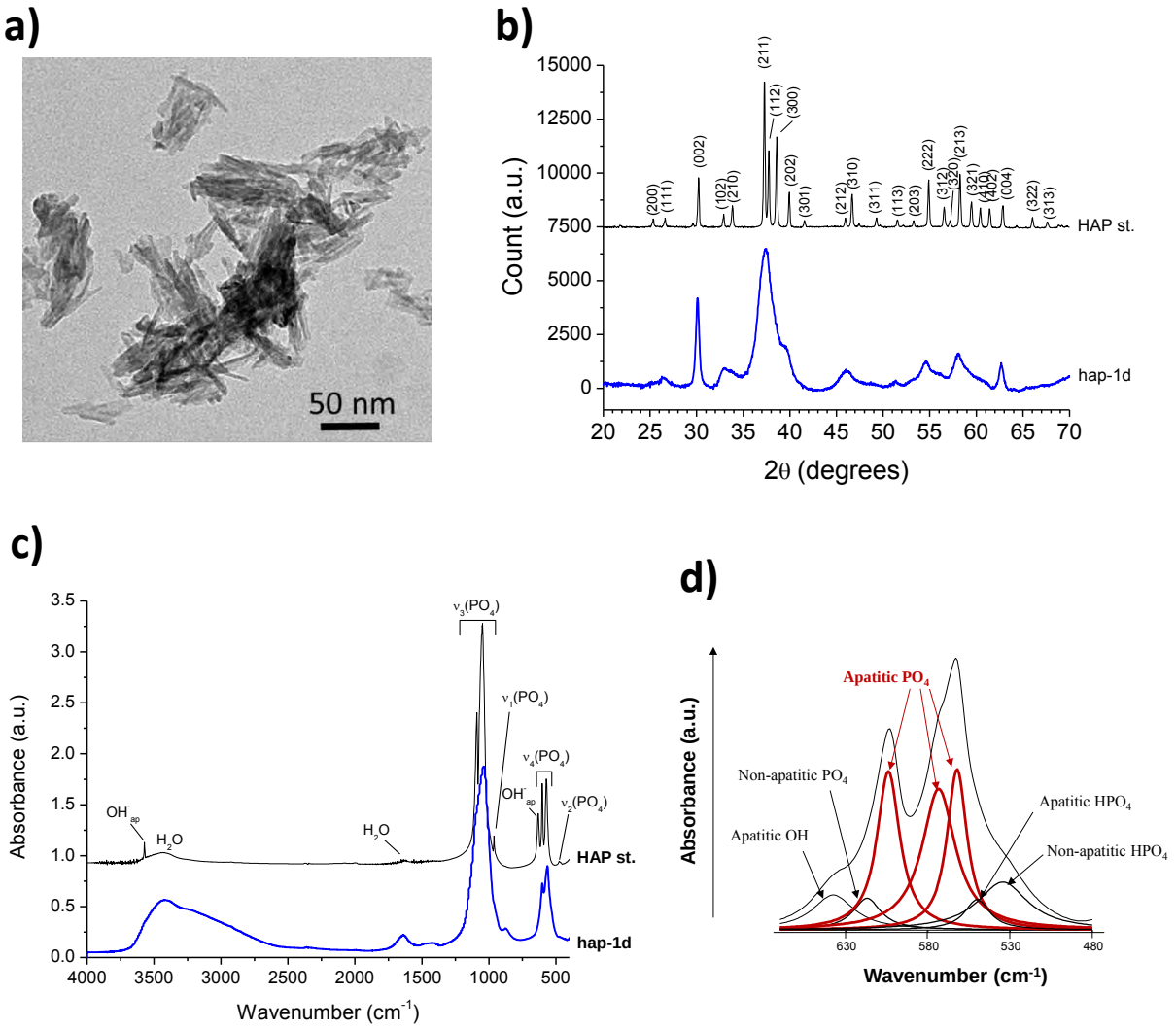

This is a preprint, the final version is subject to change, of the American Mineralogist (MSA)
Cite as Authors (Year) Title. American Mineralogist, in press.
DOI: https://doi.org/10.2138/am-2018-6415

1101 Figure 3: Schematic representation of an apatite nanocrystal in contact with an aqueous medium (carbonate free conditions)

1102

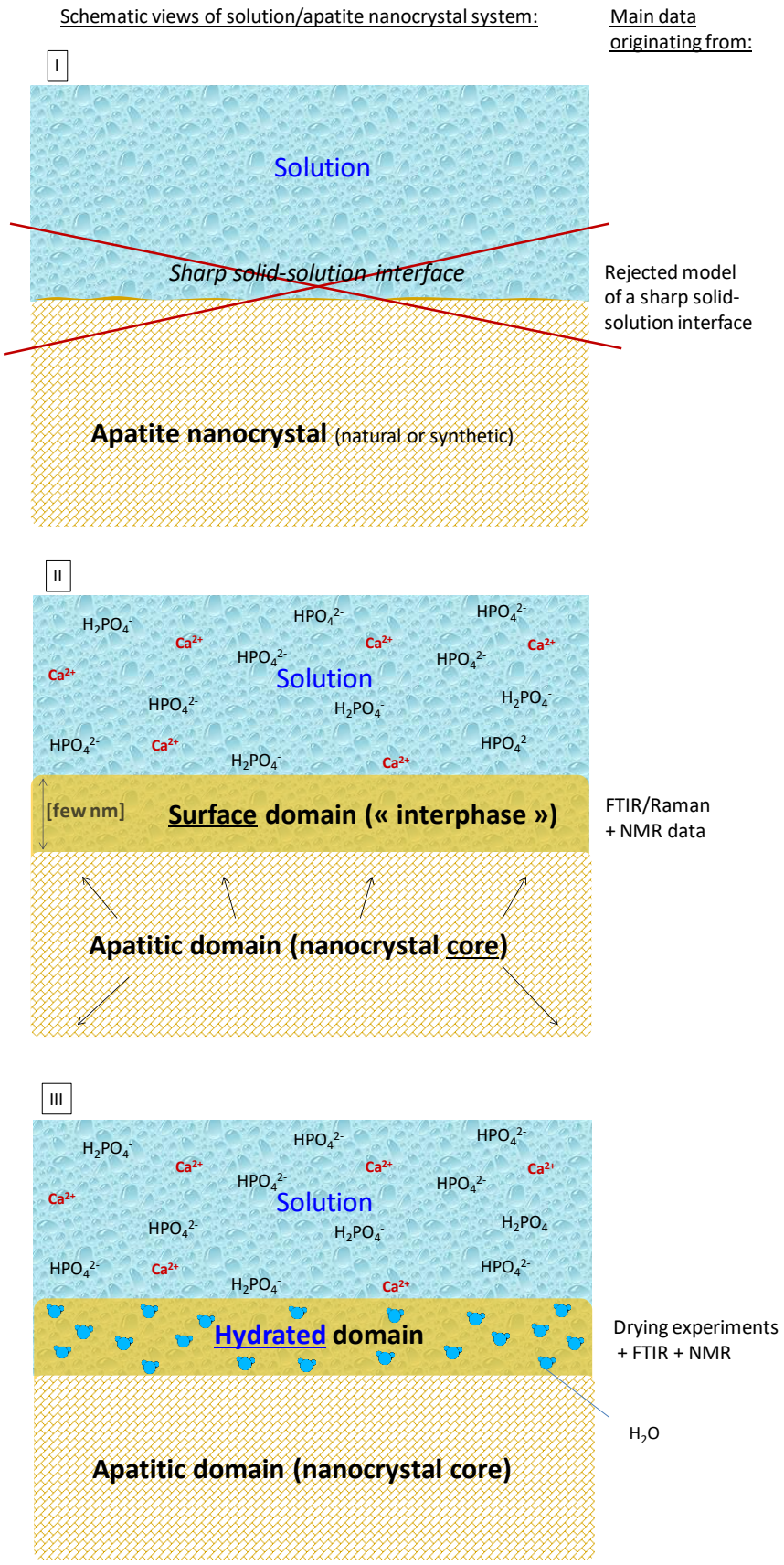

1103

1104

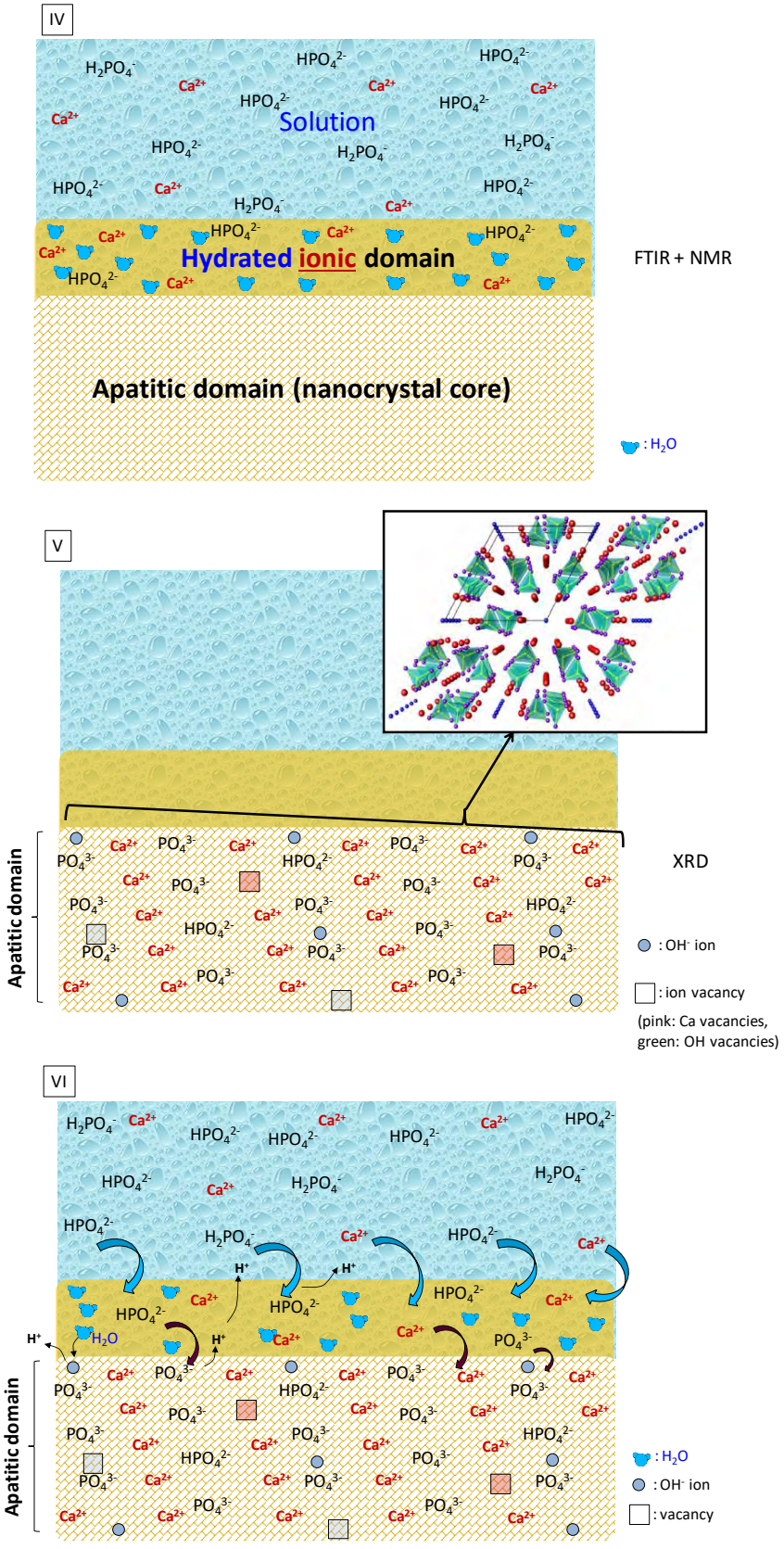

1105
1106
1107

Figure 4: Effect of apatite maturation in solution (at 22 °C) on (a) Ca/P molar ratio, (b) XRD pattern (λ_{Cu} = 1.514 Å), and (c) mean crystallite dimensions as estimated from Scherrer's formula

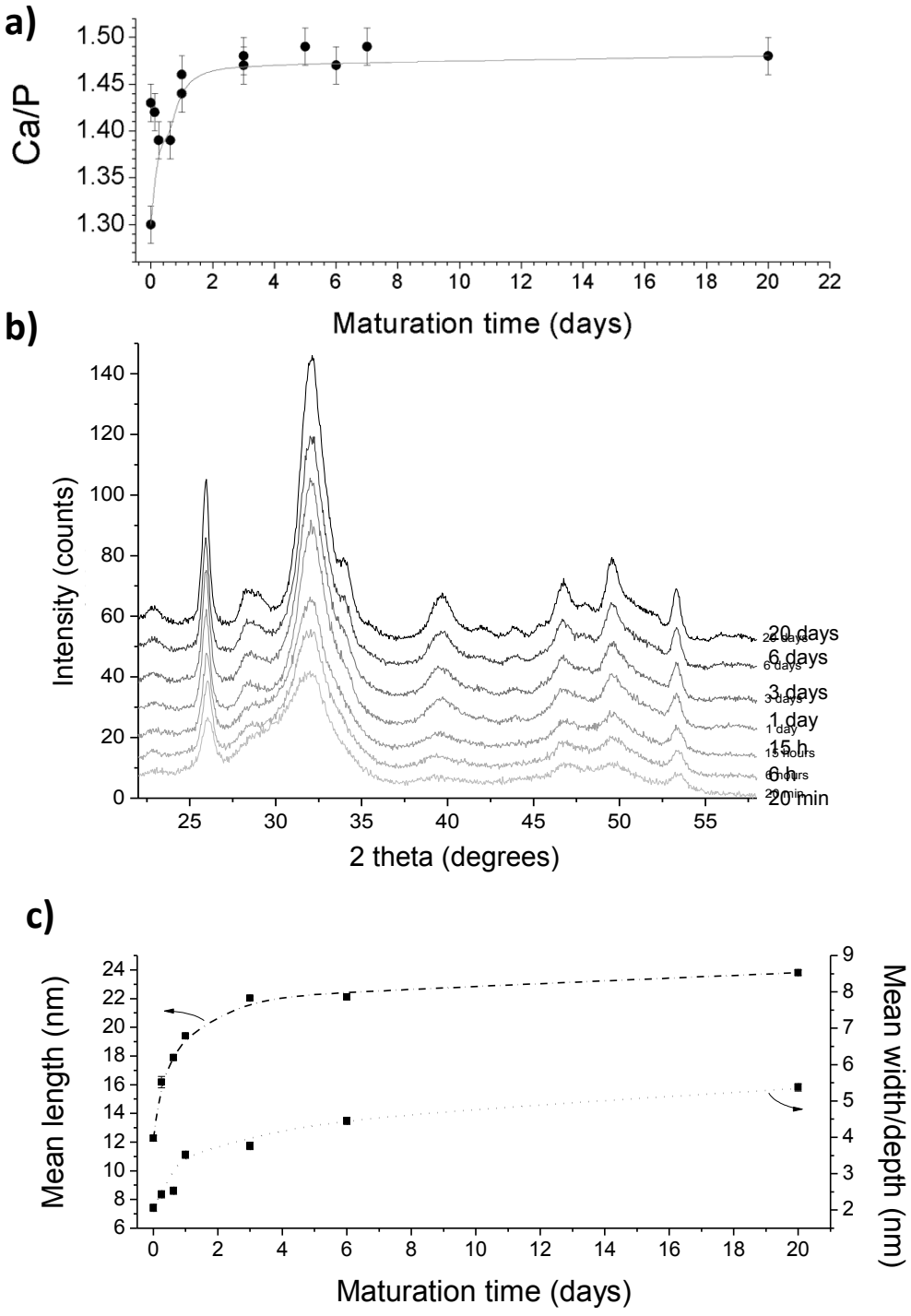

Figure 5: Evolution of ionic contents of nanocrystalline apatites versus maturation (at 22 °C): (a) Ca^{2+} and OH^- contents per unit formula and (b) example of H_2O content per unit formula (as measured from TGA for one given set of batches freeze-dried for 3 days) and evolution of non-apatitic HPO_4^{2-} environments (in relative proportion from FTIR analysis of the $\nu_4(PO_4)$ band: peak area ratio between non-apatitic HPO_4 band at 534 cm^{-1} and overall $\nu_4(PO_4)$ band area)

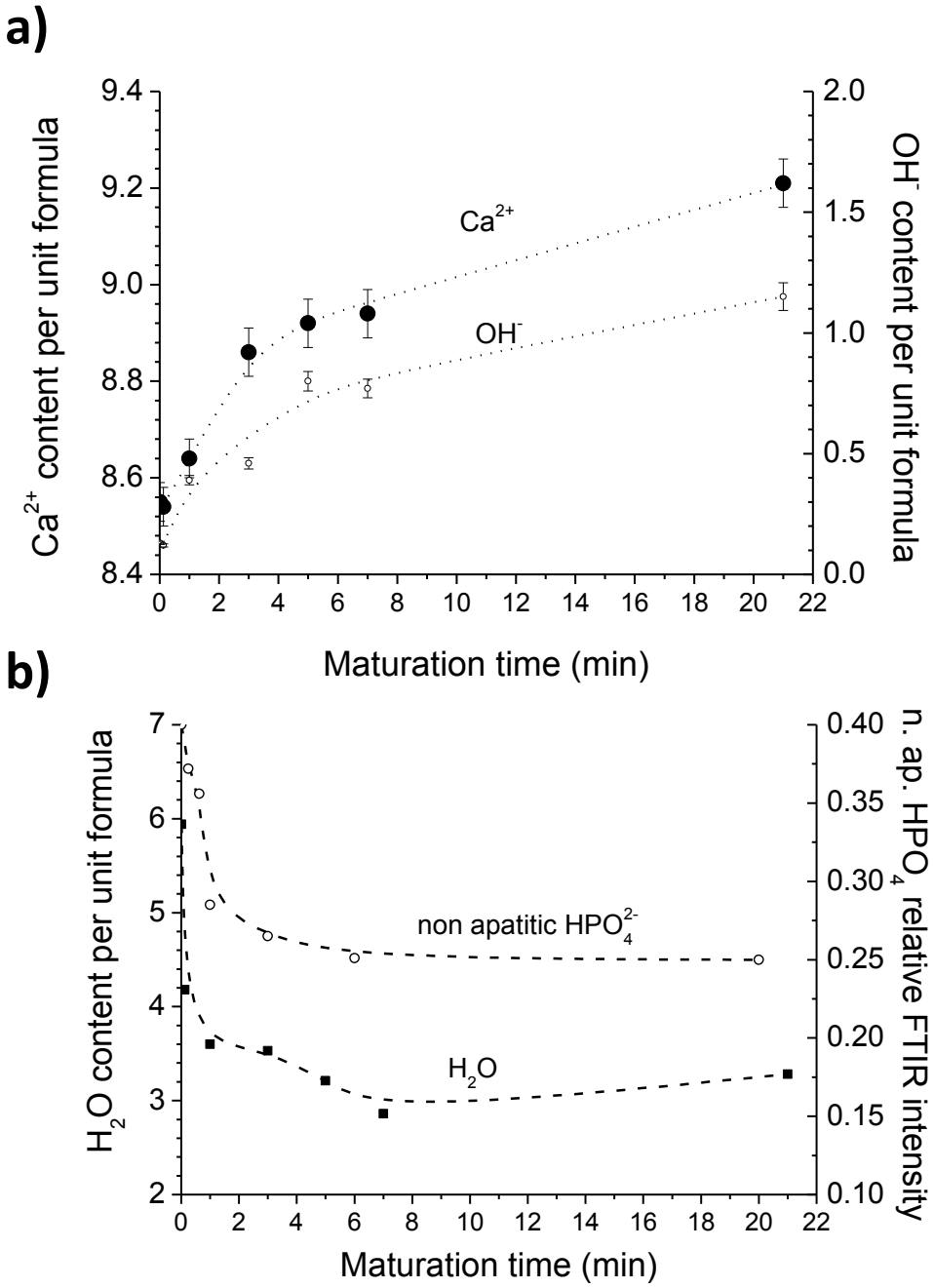

1125 Figure 6: General scheme for apatite maturation in solution (carbonate-free conditions)
1126
1127
1128

The maturation process from a chemical viewpoint:

- Evolution towards stoichiometry: **incorporating Ca^{2+} and phosphate ions from the hydrated layer** (Ca more than phosphates; Ca/P ↗)

-Release of protons in the hydrated layer + excess phosphates lead to a release $H_2PO_4^-$ into the solution (acidification)

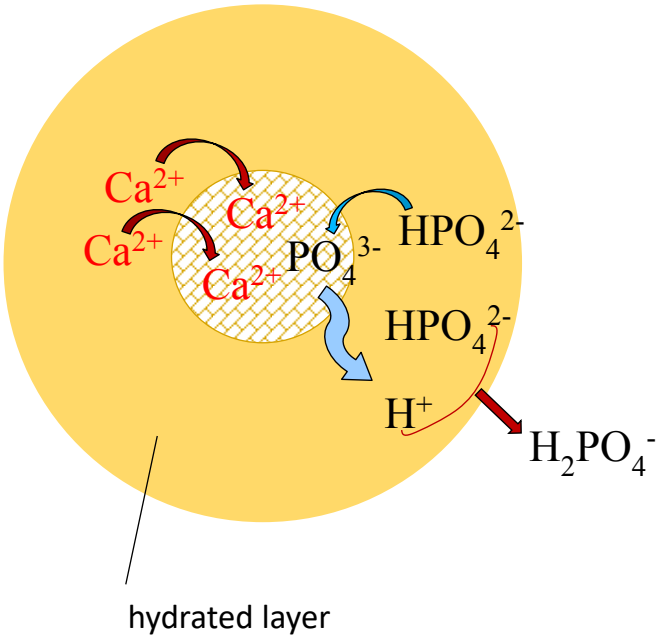

1129
1130

This is a preprint, the final version is subject to change, of the American Mineralogist (MSA)
Cite as Authors (Year) Title. American Mineralogist, in press.
DOI: https://doi.org/10.2138/am-2018-6415

Figure 7: Effect of drying on the $\nu_3(PO_4)$ domain as followed by FTIR spectroscopy for a nanocrystalline apatite sample matured few min at 20 °C

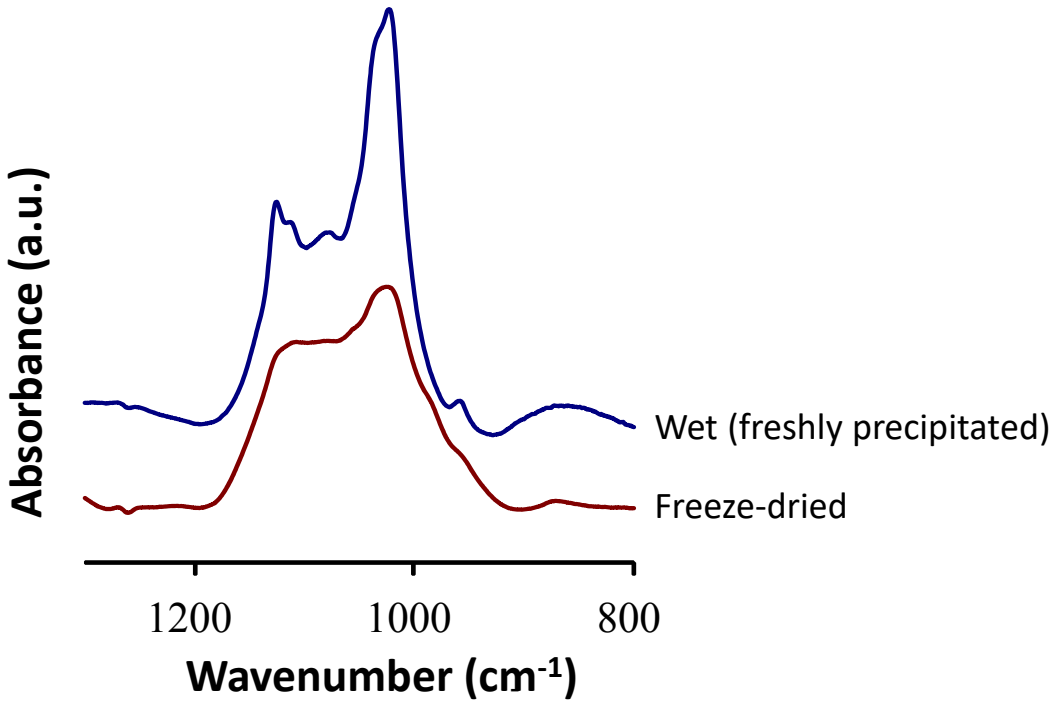

This is a preprint, the final version is subject to change, of the American Mineralogist (MSA)
Cite as Authors (Year) Title. American Mineralogist, in press.
DOI: https://doi.org/10.2138/am-2018-6415

Figure 8: a) DSC signal upon heating (at 10 °C/min) nanocrystalline apatites of various maturation times from -50 to 300 °C under nitrogen flow. Curves have been shifted intentionally to facilitate the reading. b) Example of deconvolution of DSC signal for nanocrystalline apatite matured for one day (hap-1 day)

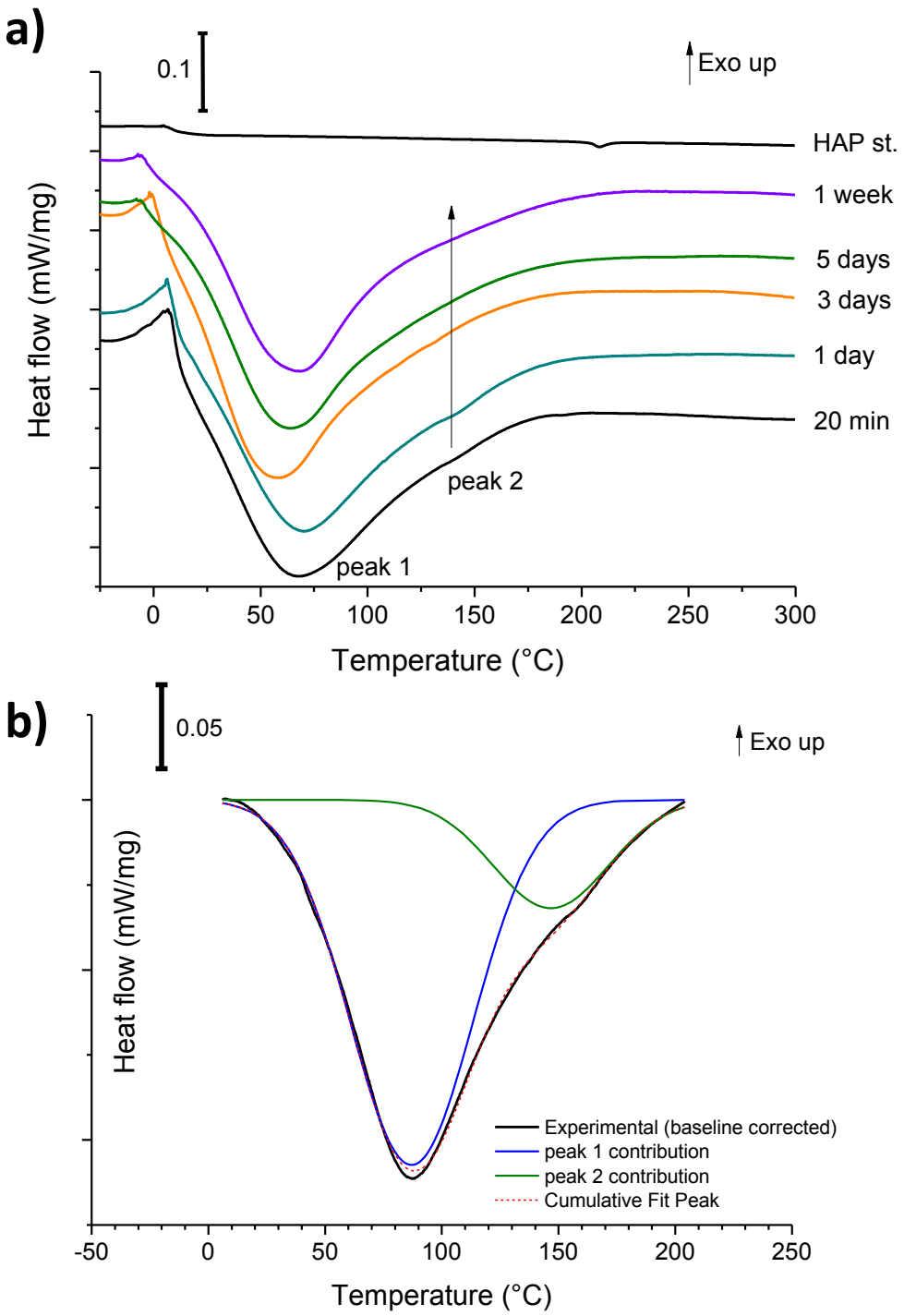

This is a preprint, the final version is subject to change, of the American Mineralogist (MSA)
Cite as Authors (Year) Title. American Mineralogist, in press.
DOI: https://doi.org/10.2138/am-2018-6415

Figure 9: Evolution of $n_1(H_2O)$ and $n_2(H_2O)$ as evaluated from DSC data: a) for samples with increasing maturation times and b) effect of re-exposure to atmosphere on sample hap-1d

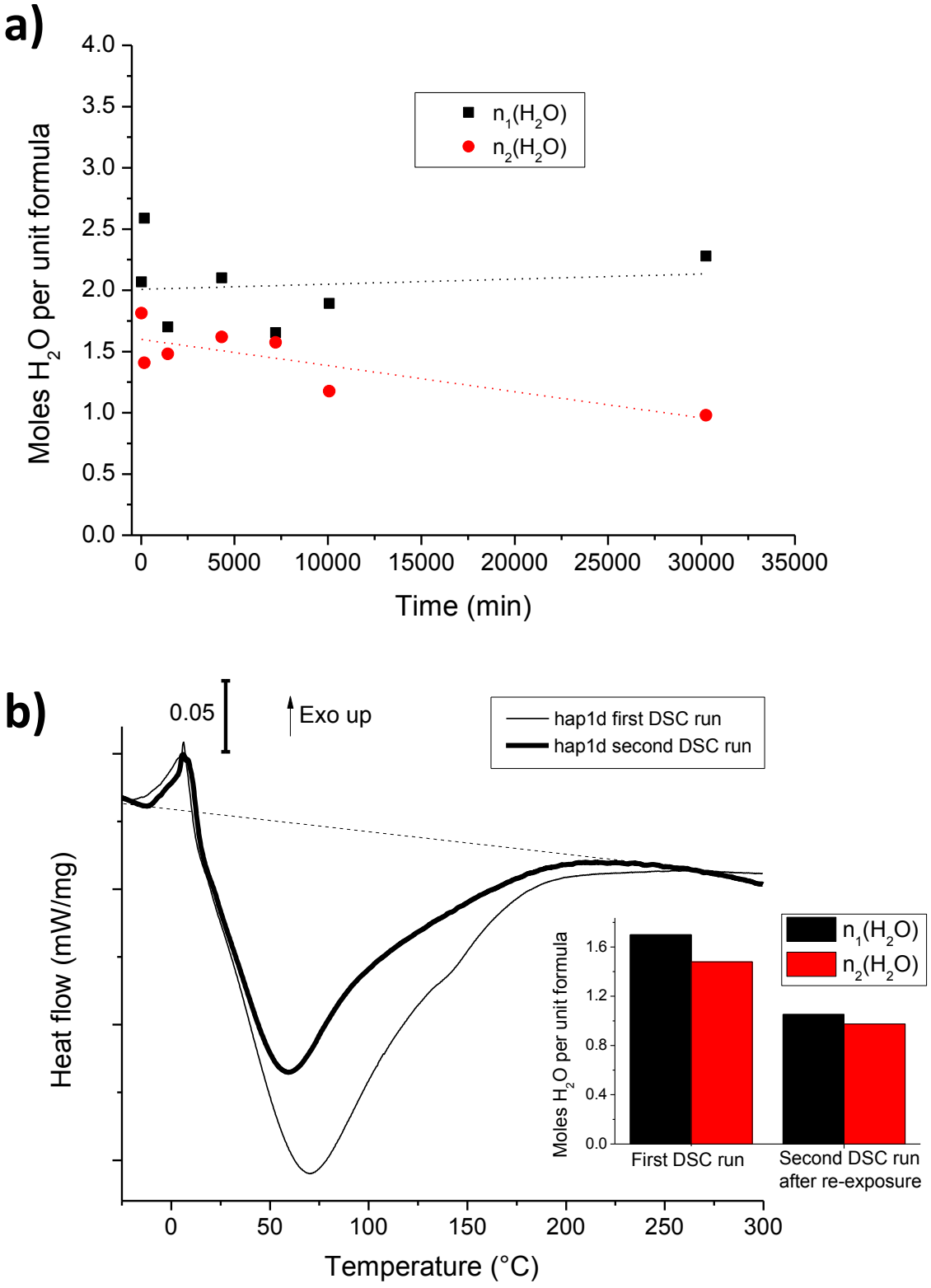

Figure 10: Cryo-FEG-SEM observations of nanocrystalline apatites matured at 25 °C between 1 min and 1 week and directly analyzed (initial magnification: x 150 000), and schematic representation of the evolutional change of morphology

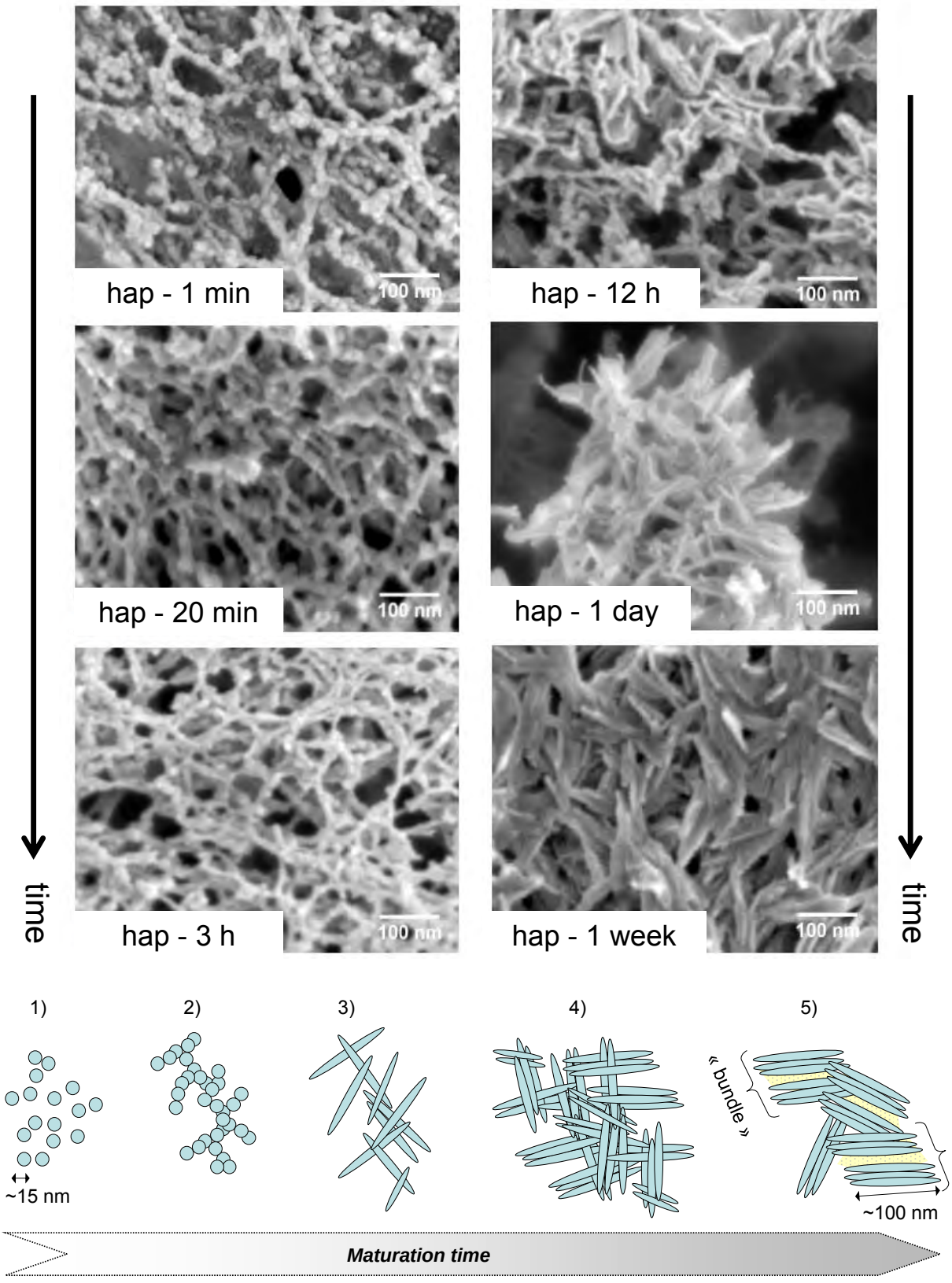

This is a preprint, the final version is subject to change, of the American Mineralogist (MSA)
Cite as Authors (Year) Title. American Mineralogist, in press.
DOI: https://doi.org/10.2138/am-2018-6415

patites with increasing maturation

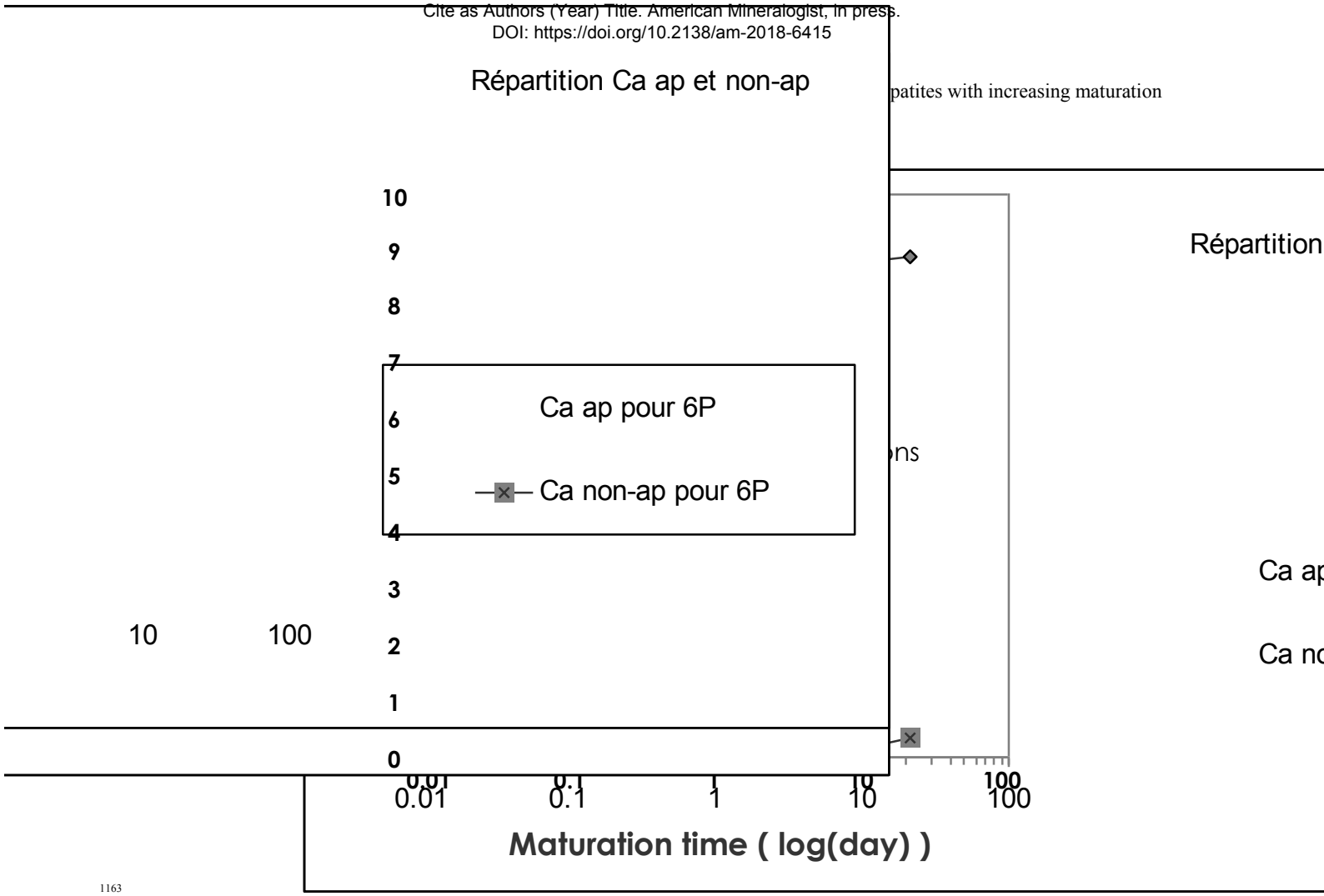

1163
1164